JGR Solid Earth

RESEARCH ARTICLE
10.1029/2021JB022615

The Effect of Authigenic Clays on Fault Zone Permeability

N. J. C. Farrell[1], N. Debenham[2], L. Wilson[3,4], M. J. Wilson[3,4], D. Healy[4], R. C. King[5], S. P. Holford[6], and C. W. Taylor[4]

[1]Rock Deformation Laboratory, Department of Earth and Environmental Sciences, University of Manchester, Manchester, UK, [2]Exxon Mobil, Melbourne, VIC, Australia, [3]The James Hutton Institute, Aberdeen, UK, [4]Department of Geology and Geophysics, University of Aberdeen, Aberdeen, UK, [5]Centre for Tectonics, Resources and Exploration (TRaX), School of Physical Sciences, University of Adelaide, Adelaide, SA, Australia, [6]Australian School of Petroleum, University of Adelaide, Adelaide, SA, Australia

Key Points:

- Tectonically deformed authigenic clays have been identified in faulted sandstones
- The morphology, aggregate structure and distribution of authigenic clay can contribute to *increased* permeability in faulted sandstones
- In contrast to accepted fault seal models, this study shows that clay-rich fault zone rocks can be the locus of *better* fluid-flow

Supporting Information:

Supporting Information may be found in the online version of this article.

Correspondence to:

N. J. C. Farrell,
natalie.farrell@manchester.ac.uk

Citation:

Farrell, N. J. C., Debenham, N., Wilson, L., Wilson, M. J., Healy, D., King, R. C., et al. (2021). The effect of authigenic clays on fault zone permeability. *Journal of Geophysical Research: Solid Earth*, *126*, e2021JB022615. https://doi.org/10.1029/2021JB022615

Received 21 JUN 2021
Accepted 30 SEP 2021

Abstract

Clays are understood to form the majority of fluid-flow barriers in faulted reservoirs and numerous fault gouge and fault seal studies have quantified the volumes of smeared and abraded clays create fluid-flow barriers along fault surfaces. However, clay-related permeability adjacent to the fault surface, including in the fault damage zone, has largely been neglected. Previous studies have shown the morphology and distribution of unfaulted authigenic clays, and not just clay volume, exert a significant control on the magnitude of permeability. However, fault-related studies have neither characterized deformed authigenic clays nor addressed their influence on fluid-flow. In this study laboratory permeabilities of faulted, authigenic clay bearing sandstones sampled from the Otway basin (Australia) and the Orcadian basin (UK) present trends which; (a) do not correspond to expected patterns of fluid-flow in faulted clay-bearing sandstones and, (b) cannot be explained using published models of permeability related to changing clay volume. Microscopic analysis shows that faulting has disaggregated authigenic clays and, similarly to framework grain deformation, comminuted and sheared clay grains. However, instead of impeding fluid-flow, analysis of pore networks (using mercury injection porosimetry) showed that faulting of authigenic clays has *increased* pore connectivity, contributing to *increased* magnitude of permeability and development of permeability anisotropy. Contrary to published results of faulting and fluid-flow in impure sandstones, our results show that fault related processes involving the formation of clays in the fault zone can *increase* permeability and *reduce* the capillary threshold pressures of fault rocks relative to the unfaulted host rock.

Plain Language Summary

Predictions of fluid leakage in geological reservoirs are essential for energy extraction (e.g., geothermal, hydrocarbons), development and maintenance of sustainable energy resources (e.g., carbon dioxide sequestration and nuclear waste storage). Reservoir-bounding faults commonly form fluid-flow barriers as the process of faulting breaks grains and smears clays along fault surfaces creating a seal. Therefore, the volume of clay in faulted rocks is an important parameter in relation to fault sealing capacity. Authigenic clays are minerals that commonly grow in spaces between grains, choking fluid pathways and reducing flow. In this study, microscopic analysis of two faulted sandstones containing authigenic minerals (chlorite and kaolinite) showed that faulting also breaks authigenic clay grains. However, instead of impeding fluid-flow, laboratory measurements of faulted sandstones showed that deformation of authigenic minerals can influence flow direction and even increase the magnitude of fluid-flow. Consequently, rather than representing fluid barriers, some faults may actually form important fluid draining structures. These novel results prompt questions about the robustness of parameters currently used to model fluid-flow around faults and, with global need for sustainable energy demanding that we can safely store fluids in subsurface reservoirs, should motivate geologists to take a fresh look at fault seal analysis.

1. Introduction

Faults exert a major control over the movement and containment of fluids. The role of smeared, disaggregated or injected clay grains along the surfaces of faults and their role in reducing permeability and creating hydraulic barriers or seals has been extensively researched (Childs et al., 1997; Eichhubl et al., 2005; Fisher

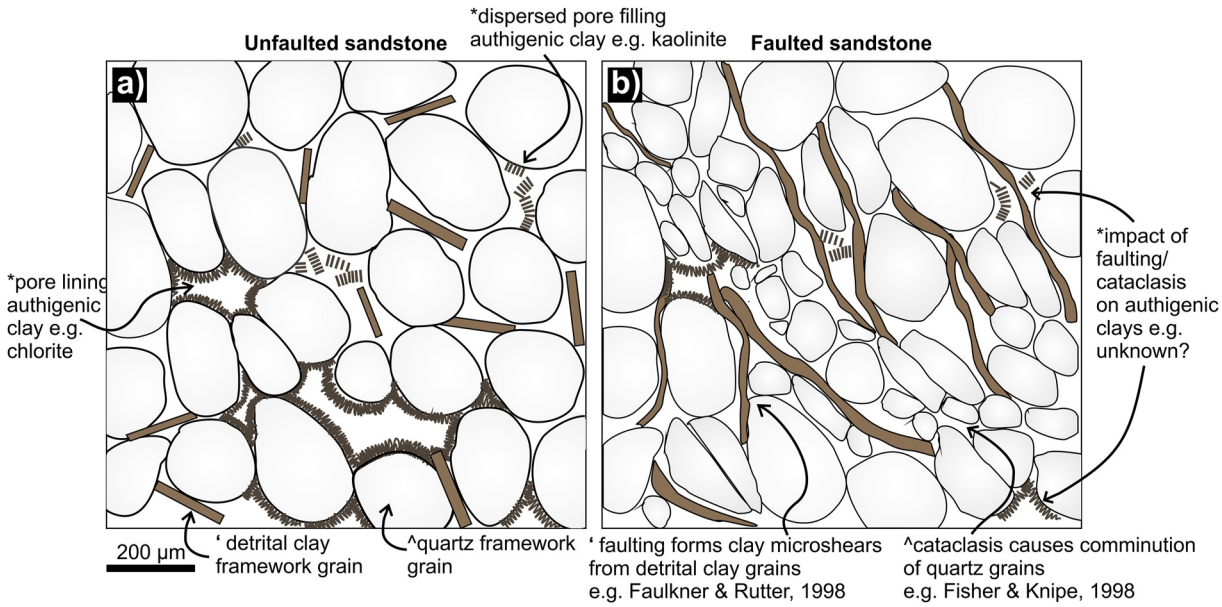

Figure 1. Current model for how deformation of impure sandstone (e.g., containing phyllosilicates) changes the rock microstructure to form fault seals (after Jolley et al., 2007). (a) Unfaulted impure sandstone containing quartz and detrital clay framework grains and authigenic pore lining and pore-filling clays. (b) Fault induced cataclasis and shearing deforms grains and forms low-permeability clay microshears. The effects of deformation on the morphology and distribution of authigenic clays is unstudied.

& Knipe, 1998; Freeman et al., 1998; Fristad et al., 1997; Knipe, 1997; Knott, 1993; Lindsay et al., 1993; Manzocchi et al., 1999; Moore & Reynolds, 1989; Rempe et al., 2018; Vrolijk et al., 2016; Yielding, 2002; Yielding et al., 1997). However, the role of clays in controlling permeability adjacent to fault surfaces, including in fault damage zones, has largely been neglected. In faulted granular rocks, deformation and cataclasis of framework grains and subsequent alteration of pore networks (i.e., pore throat distributions and pore orientations) in fault damage zones have been shown to form both flow barriers (Fisher & Knipe, 1998; Yielding et al., 1997) and flow conduits (Farrell et al., 2014; Morrow et al., 1984). Farrell et al. (2014) also showed that deformation mechanisms can create anisotropic permeability. There is ample evidence for fluid infiltration in faulted rocks (e.g., pressure solution, vein mineralization, clay precipitation) but fewer explanations of the processes that create the necessary conduits for these fluids.

Permeability, a proxy for conductivity, is the result of a complex interplay of the nature of fluid types, the pressure gradients on these fluids, and material properties through which the fluids move. Although volumetrically trivial, it is well documented that pore throat properties are a fundamental control on the magnitude of permeability. Matrix grains, such as pore lining clays, are a key constraint on both the *aperture* and *openness* of pore throats. However, deformation of matrix grains within the pore networks, and specifically the impact of clay grain cataclasis on fluid-flow around fault zones, is unknown. A few studies have attempted to quantify the effect of fault deformation on matrix grains that commonly congest pores and plug pore throats, e.g., authigenic clays (Haines et al., 2009; Lommatzsch et al., 2015), but none have measured the effects of authigenic clay deformation on fault zone permeability. In sedimentological studies (i.e., unfaulted sandstones), the negative effects of small volumes (<10%) of authigenic clay which fill/line the inside of pores and pore throats, and the impact of variable clay morphologies on fluid-flow are well-established (Howard, 1992; Pallatt et al., 1984; Neasham, 1977 and Wilson & Pittman, 1977 respectively). Migration of small volumes (commonly <10%) of non-swelling, dispersible clay particles which choke pore throats in sandstone reservoirs is the most common mechanism of "formation damage." This is a substantial problem in the hydrocarbon industry where fines migration, resulting from fluid injection, can impact both drilling and production, directly affecting the economic viability of reservoirs (Schlumberger, 2016). However, perhaps due to their relatively tiny volumes, the effect of deformed (cataclased) authigenic clays on the hydraulic behavior of fault zones is unstudied (Figure 1).

Hydraulic conductivity is a complex function of multi-scale properties of a porous medium ranging from the size and distribution of lithological bodies and faults, through the grain, pore and microcrack fabrics of rocks, and down to the interface wettability and electrical potential of mineral surfaces. Critically, the net effect of these properties on permeability (which is also a function of pore fluid properties) are not directly proportional to their magnitude. In rocks containing pore-filling authigenic clays, the smallest volumes can often have the greatest affect: e.g., pore throats may only account for <0.1% of the total volume. This study presents data on the morphology, aggregate structure and distribution of authigenic clays in sandstone-hosted fault zones and explores the impact of deformation of both pore-lining and pore-filling clays on fault zone permeabilities.

1.1. Influence of Authigenic Clay Volume and Distribution on Permeability

Authigenic clays are formed by diagenetic alteration of *in situ* minerals in impure (e.g., arkosic sandstones, lithic arenites) and have been identified in 90% of sandstones (from a study of 785 sandstones, Wilson & Pittman, 1977). Authigenic clays precipitate within pore spaces and, although relatively minor in volume (<10%), they have been shown to significantly decrease pore connectivity and permeability by over five fold (Bjørlykke and Jahren, 1992; De Waal et al., 1988; Howard, 1992; Hurst & Nadeau, 1995; Pallatt et al., 1984; Stalder, 1973; Thomas, 1978; Wilson et al., 2013; Wilson & Pittman, 1977; Worden & Morad, 1999). Mechanisms for permeability reduction due to pore filling clays are: Precipitation of authigenic clays within the pore space which dominantly constrict pore throats (Wilson & Pittman, 1977); complex pore filling morphologies which reduce the effective porosity (porosity that contributes to permeability) by creating microporosity (Nadeau & Hurst, 1991); and porosity reduction due to the formation of water shell on the clay surfaces creating a double electric layer (DEL) and diffuse layer (Derjaguin et al., 1987).

In the hydrocarbon industry the negative relationships between volume, type and distribution of authigenic clays and permeability are well-documented (Bushell, 1986; De Waal et al., 1988; Heaviside & Black, 1983; and Pallatt et al., 1984). There are many studies highlighting the discrepancy between derived permeabilities depending on the sample preparation methods (e.g., De Waal et al., 1988; Kantorowicz, 1990; Nadeau, 1998). Accurate determination of the effect of clay precipitation on permeability is problematic because in natural rocks which have undergone the same burial and diagenesis there is rarely a clay-free sample to compare with. Previous studies have attempted to isolate the effects of authigenic clays on permeability by: (a) destruction of authigenic clays; (b) modeling of clay-free sandstones; and (c) production of synthetic sandstones containing clays and without clays. Results of these studies are summarized in the Supporting Information S1.

1.2. Influence of Authigenic Clay Mineralogy on Permeability

In addition to analysis of authigenic clay volume and distribution on permeability, studies that quantified fluid-flow in unfaulted sandstones containing authigenic clays have shown that difference in clay type can alter permeability. Synthesis of data from these studies shows gas permeabilities varied over four orders of magnitude (2.9×10^{-17}–2×10^{-13} m^2) for samples that contained 10% volume of different clays including kaolinite, illite, chlorite and montmorillonite (Figure 2a, box 1) (Milliken, 2001; Neasham, 1977; Pike, 1981). This data set also shows gas permeabilities ranged over four orders of magnitude (1.5×10^{-16}–1.5×10^{-12} m^2) for samples that contained similar amounts of authigenic kaolinite (Figure 2a, box 2). Samples with equal porosities but differing authigenic clay types, also varied in permeability over four orders of magnitude (9.86×10^{-17}–4.4×10^{-13} m^2) (after Neasham, 1977) (Figure 2b, box 4). Furthermore, sandstones that contained authigenic illite with similar porosities also varied over four orders of magnitude (3.9×10^{-17}–1.18×10^{-13} m^2) (Figure 2b, box 5) which shows that although authigenic clays do not control the permeability, they are responsible for a substantial amount of scatter. Moreover, in some cases, the varying morphologies of the clays and their characteristic distribution within pores, that is, dispersed, pore bridging or pore lining, can have the greatest effect on permeability (Neasham, 1977).

Previous fault zone studies on the hydraulic properties of "phyllosilicate framework fault rock" formed in impure sandstones (Fisher & Knipe, 1998; Sperrevik et al., 2000) have shown barriers to flow produced by disaggregation and redistribution of framework clays (Knipe, 1992) or networks of clay microshears

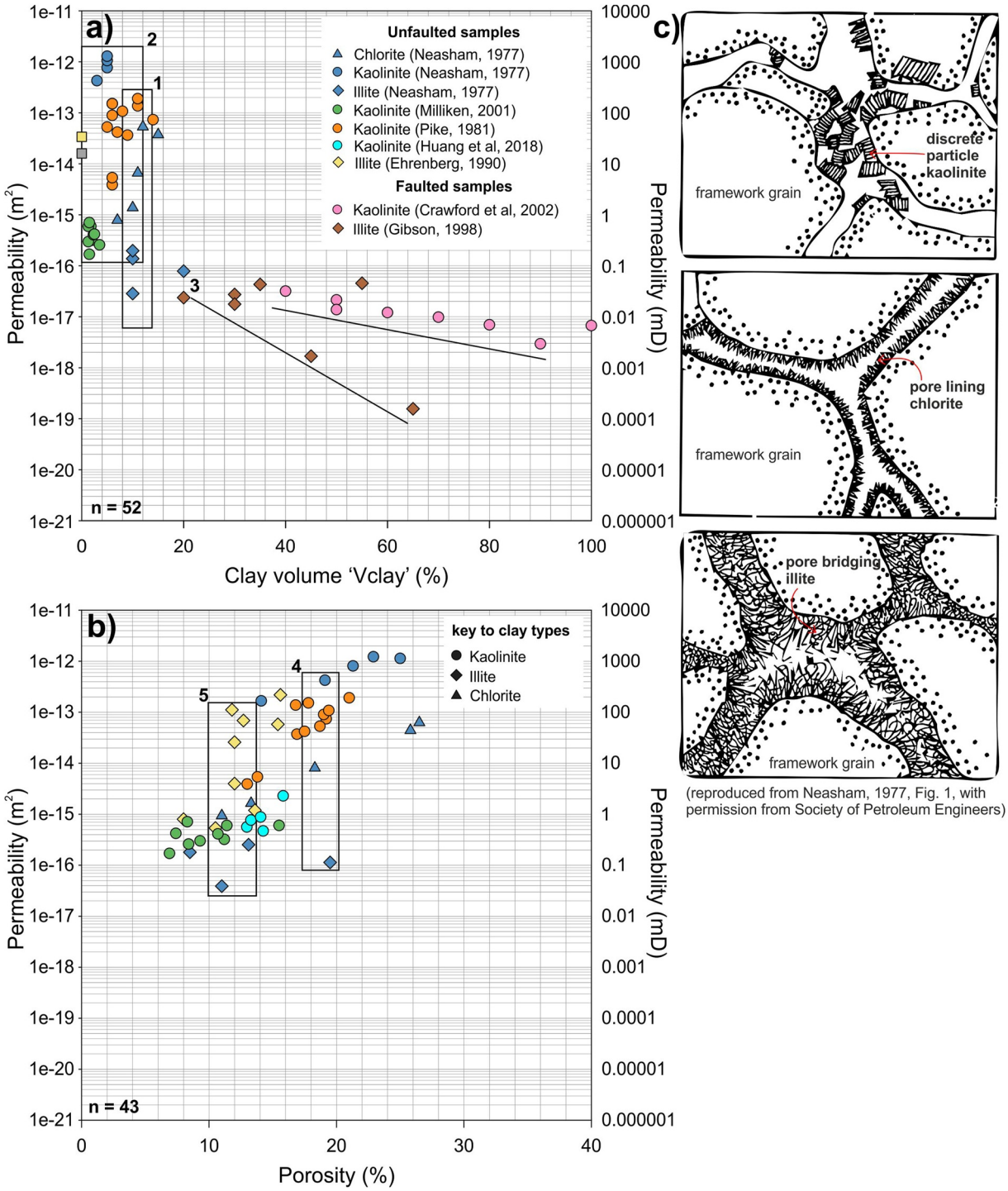

(reproduced from Neasham, 1977, Fig. 1, with permission from Society of Petroleum Engineers)

Figure 2. Gas permeabilities measured in unfaulted and experimentally faulted core plugs that contained different clay types at (a) varied volumes and (b) varied porosities alongside illustrations of typical morphologies of unfaulted authigenic clays reproduced from Neasham, 1977 (c). (a) Data reproduced from seven published studies showing that: (i) Permeability ranged over five orders of magnitude for unfaulted samples containing ~10% volume of different clays, including kaolinite, illite and chlorite, (ii) permeability ranged over four orders of magnitude in samples with similar volumes of kaolinite, (iii) gas permeabilities of experimentally faulted samples of kaolinite and illite both decreased with increased clay volumes, but at different rates. (b) Data reproduced from five published studies showing that, (iv) permeabilities ranged over four orders of magnitude in samples with porosities ~19% but containing different authigenic clays including illite, chlorite, kaolinite, (v) permeabilities ranged over four orders of magnitude in samples with porosities all between 11% and 14% all containing authigenic illite.

(Faulkner & Rutter, 1998). However, in these studies, *conduits* to flow, which may have formed by disaggregation and cataclasis of pore throat blocking authigenic clays, were not discussed (Figure 1). Experimental work has synthesized the formation of clay fabrics induced by faulting using shear loading apparatus to investigate the relationships between clay volume, deformation fabric and liquid and gas permeabilities (Crawford et al., 2008; Haines et al., 2009; Zhang & Cox, 2000). These studies showed that increased quantities of clay (from 20% to 100%) reduced permeability and that the volume of clay, rather than the amount of deformation (via shearing), was a greater control on the resultant permeability (Crawford et al., 2008). Gas permeability from shear experiments on gouges with similar clay volumes, but different mineralogies (see Figure 2, box 3), exhibited lower permeabilities for illite gouges (Gibson, 1998) than kaolinite gouges (Crawford et al., 2008). Although these studies focused mainly on the permeability of clay fabrics produced by comminution and shearing of phyllosilicate framework grains (and did not discuss alteration of pre-existing authigenic clays in the pore network), these results showed that clay mineralogy can exert an important influence on permeability in faulted and unfaulted rocks.

1.3. Improving Fault Seal Models

Most previous models for predicting fault zone permeability/transmissivity use purely mechanical or geometric mixing models, due in large part to the fact that fault throw and stratal thickness are easier to determine in subsurface formations e.g., shale smear factor (SSF; Lindsay et al., 1993), shale gouge ratio (SGR; Yielding, 2002), or clay smear potential (CSP; Fulljames et al., 1997). While useful, these models assume that increased clay volume produces lower permeability rocks and do not account for the measured variable effects of authigenic clay composition (Neasham, 1977) or the effects of intrafault diagenesis (Laubach et al., 2014). Authigenic clay type is often related to burial depth and temperature (Bjørlykke and Jahren, 1992; Lanson et al., 2002) and can be inferred to explain data scatter in previous studies of permeability versus clay volume. For example, a study of North Sea fault rocks in phyllosilicate-framework/impure sandstones showed a weak negative relationship of water permeability and clay content with permeabilities ranged over seven orders of magnitude for samples with similar clay volumes (Sperrevik, et al., 2000) (Figure 3). Highest permeabilities were from shallow buried rocks (<2,500 m) and the lowest permeabilities were from deeply buried rocks (>3,600 m). Although Sperrevik's study did not document the type of clay present in the samples, shallow depths (<2,500 m) are favorable for the formation of kaolinite (from meteoric water and Al-rich silicates) while depths >3,000 m correspond to formation of illite (from reactions between kaolinite and K-feldspar) (Bjørlykke, 1998) and smectite to illite transition (Lanson et al., 2009). At depths greater than 4,000 m the morphology of illite can change with lath-shaped crystals increasing in size and becoming pseudo-hexagonal (Lanson et al., 2002). Pore bridging distribution of illite has a larger negative effect on permeability compared to the dispersed distribution of kaolinite (Neasham, 1977) (Figure 1), so clay type could be an important parameter in explaining the permeability data scatter in this study.

Analysis of previous fault permeability studies shows that a full understanding of hydraulic properties of faulted impure sandstones requires consideration of the whole rock microstructure (i.e., pore-filling grains as well as framework grains) and its relationship to mechanical and chemical fault deformation processes. This requires integration of petrophysical data to define hydraulic trends and pore connectivity, microstructural analysis of pore and grain morphology and chemical analysis of clay types. In this study, we hypothesize that fault related changes in morphology and distribution of authigenic clays will alter the hydraulic conductivity of sandstones and influence the permeability patterns in the fault damage zone. The study objectives are to: (a) Investigate how authigenic clays were altered and/or generated during fault deformation; and (2) quantify permeabilities in variably deformed samples with differing clay characteristics.

To test the hypothesis, laboratory petrophysical tests were conducted on core plugs sampled around two inverted normal faults of a scale that are visible in a seismic reflection profile. In the North Scapa Fault (Orkney, UK) damage zone sandstones contain authigenic kaolinite, while at the Castle Cove Fault in Victoria (Australia), damage zone sandstones contain authigenic chlorite. Previous analysis of these two samples suites have shown relationships between fault rock pore fabric and anisotropic permeability (Farrell & Healy, 2017) and increasing porosity and permeability (Debenham et al., 2019). However, although these papers both noted changes in authigenic clay distributions with increased fault related deformation, they did not document or quantify the profound effect that even minor amounts of pore and throat filling

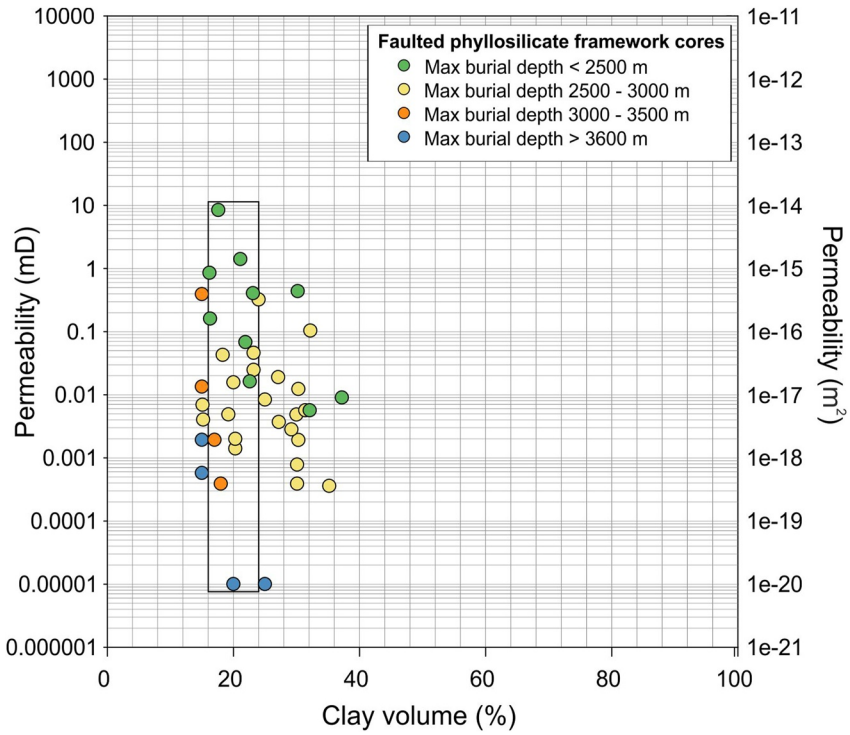

Figure 3. Graph showing water permeabilities of impure sandstones with varying clay volumes, measured in core plugs by Sperrevik et al. (2000).

authigenic clay can have on sandstone properties (Wilson & Pittman, 1977). Therefore, they did not investigate the potential role of faulted authigenic clay in contributing to the reported pore size and shape changes that dominated permeability trends. Our results show that faulted sandstones with deformed authigenic clays: (a) Do not correspond to widely accepted patterns of permeability and fault deformation; and (b) cannot be explained solely by fault-related development of anisotropic grain, pore or microcrack fabrics, or by a simple factor of clay volume.

2. Methods

2.1. Petrographic Analysis and Mineralogy

Qualitative and quantitative analysis of rock microstructure and mineralogy was conducted using scanning electron microscopy (SEM) and X-ray diffraction (XRD). The size, distribution and morphology of clays were characterized from secondary electron (SE) images taken of chips of rock (sampled from the ends of core plugs) on a Zeiss Gemini SEM 300 high-resolution Field Emission Scanning Electron Microscope (FESEM). Images were taken at a range of magnifications between 100–3,000X using a low accelerating voltage of 5 kV. Clay types were identified on SE images using energy-dispersive X-ray spectroscopy (EDS) point analysis in an SEM. Quantification of bulk rock mineralogy ("whole rock") and clay fraction ("clay volume") was completed using XRD analysis on powdered samples. XRD analysis was carried out on 10 samples selected from varying distances from the fault surfaces. Results were interpreted using the Rietveld method (1967). Details on XRD sample preparation techniques and analysis methods can be found in the Supporting Information S1.

2.2. Petrophysical Analysis

Connected porosity was measured in the core plugs using a helium (He) porosimeter at room temperature. Core plugs were put into a tight compartment and a known volume of He gas was injected from a separate chamber at 0.689 MPa. The resulting lower pressure in the core plug chamber was recorded and then an

equilibrium pressure of the two chambers was calculated using Boyle's Law. Porosity was then derived from the core plug grain volume subtracted from the bulk volume - calculated from the caliper dimensions of the core plug.

Gas permeabilities were measured using the steady state, constant flowrate method on a Jones permeameter at 2.7 MPa confining pressure (as described in Jones & Owens, 1980). Tests were run at room temperatures, 18–20°C using nitrogen as a pore fluid. In order for commonly used experiments with gas to measure permeability, a correction must be made for the "slippage" effect of gas at grain boundaries. To account for gas slippage - that is, to "correct" gas permeability measurements to the permeability of a core with a liquid flowing through it–we applied a Klinkenberg correction (1941) using an equation modified from Darcy to account for using this compressible medium (after Tanikawa & Shimamoto, 2009, Equations 6 and 7).

$$k = 2\mu BQ\left(\frac{L}{A}\right)/\left(P_1\text{^}2\right) - \left(P_2\text{^}2\right) \quad (1)$$

where k = permeability (m^2), μ = viscosity (Pa s), B = atmospheric pressure (Pa), Q = gas flowrate (calculated from V/t, volume of fluid (m^3) passed in time (s^{-1})), L and A = core plug length and cross-sectional area (m and m^2, respectively), P_1 and P_2 are the input pressure and output pressure respectively (Pa). Due to the nature of the Jones permeameter (which derives flowrate from measurement of displaced Meriam oil in a flowmeter manometer) permeabilities are calculated using non-SI units (millidarcies, mD; centipoise cP; atmospheres, atm; centimeters, cm^2, cm^3) then converted to SI units. A detailed account of how we derived permeability can be found in the Supporting Information S1.

Pore connectivity was quantified using mercury injection porosimetry (MIP) on a Micromeritics Autopore IV system. This method measures the capillary pressures required to force non-wetting liquid mercury into voids in a rock sample to evaluate the sealing capacity of rocks. MIP tests were conducted on 1 cm diameter semi-circular disks of sandstone from slices of rock that had been cut from the ends of core plugs. Samples were placed inside a penetrometer (glass holder with capillary stem) and the hollow stem of the penetrometer was filled with a known volume of mercury. As mercury is non-wetting and will not soak into pore spaces ambiently, it is intruded into the pores by increasing an externally applied pressure. The volume of mercury entering the pores is measured using an electrical capacitance dilatometer and is accurate to changes in volume <0.1 μL. Pressures required to saturate pores is inversely proportional to the size of the pores, or more accurately the pore openings, known as pore throats. Therefore, pore throat sizes can be calculated using the injection pressures required to force an amount of fluid mercury into a sample against the opposing force of the mercury's surface tension using the Washburn equation (Washburn, 1921). Volume porosity for each pore class size was calculated as a fraction using the cumulative volume of mercury injected. This method assumes a density and surface tension of mercury of 13.54 g/ml and 0.485 Nm^{-2}, respectively, and a mercury-sandstone contact angle of 141°. Using this method, pore throat sizes could be measured to an accuracy of <5 nm.

3. Geological Background and Materials

Samples were collected from two outcrop examples of inverted (reverse reactivated), normal faults hosted in fluvial, impure sandstones with the aim of quantifying the petrophysical properties, microstructure and mineralogy. The two sandstone formations have differing host rock mineralogy so that we can consider the influence of original facies and pre-faulting diagenesis on the in-situ, post-faulting pore fabrics.

The North Scapa Fault is a basin-scale normal, reverse-reactivated fault (displacement >100 m, strike length >10 km) exposed at Orphir Bay (Orkney UK) (HY334042) which juxtaposes fluvial sandstone in the hanging wall against lacustrine mudstones in the footwall (Farrell & Healy, 2017; Hippler, 1993). Fluvial sandstones of the North Scapa Sandstone (of the Middle Old Red Sandstone Formation) were sampled from coastal cliff exposures at various distances (up to 100 m) from the fault surface. The North Scapa Sandstone is a fine-grained (modal grain diameter of 200 μm), well-sorted, quartz sub-arkose displaying cross bedding, and deposited in a principally fluvial environment. Mineralogy is dominated by quartz with some K-feldspar and mica grains (annotated in Figure 4a).

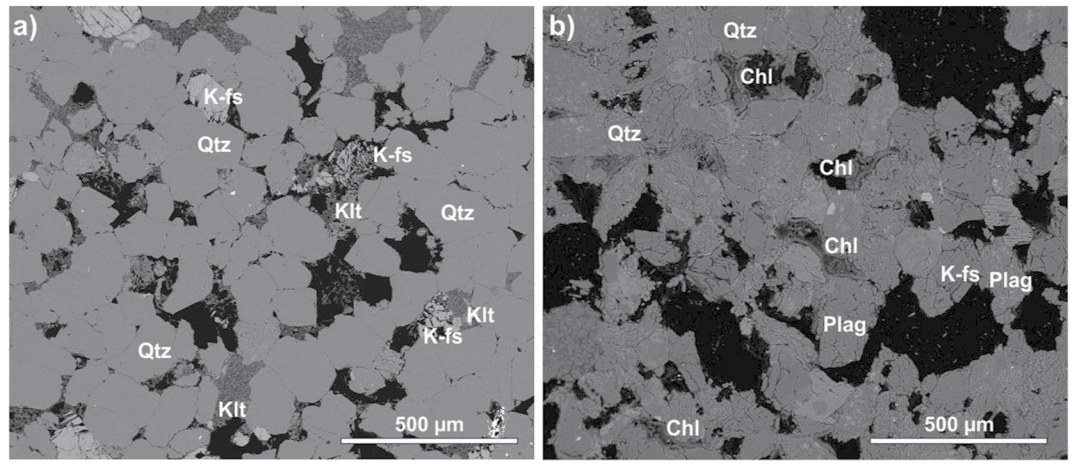

Figure 4. Back-scattered electron images depicting the microstructure and mineralogy of the North Scapa Sandstone and the Eumeralla Formation sandstone. (a) Scapa sandstone mineralogy is dominated by framework grains, quartz (Qtz), K-feldspar (K-fs) with pore-filling authigenic kaolinite clays (Klt) that have been precipitated from dissolved K-feldspar grains. (b) Eumeralla sandstone mineralogy is dominated by a framework of quartz (Qtz) and plagioclase feldspar (Plag) with pore lining chlorite clays (Chl) formed from the alteration of volcanic grains.

The sandstone has a mean porosity of 12% as quantified by helium porosimetry data. Pore size distributions are visibly bimodal comprising large, intergranular and secondary dissolution pores with jagged outlines termed "macro" pores and clusters of very small pores surrounded by authigenic kaolinite termed "micro" pores. Larger oblate pores are spatially distributed and visually unconnected (Farrell & Healy, 2017). Some pores are partially filled, some completely filled and some devoid of clay (Figure 4a). Clay volume is 3.1% comprising kaolinite and some illite (quantified by XRD analysis, Table 1). Kaolinite is authigenic in origin from the breakdown of K-feldspar as evidenced by the presence of fragments of remnant feldspar in secondary pores containing kaolinite (Figure 4a). Clays are in contact with grains but are not fixed to framework grains. Previous work on faulted samples of Scapa sandstone has shown some intergranular fractures in BSE images sampled at all proximities to the fault surface (Farrell & Healy, 2017). However - surprisingly in comparison to the macrofractures observed and quantified in the field - microfractures are not abundant

Table 1
XRD Analysis of Whole Rock Samples of Scapa and Eumeralla Sandstones to Determine Percentage Weight by Mineral Phase

Scapa sandstone		XRD analysis (whole rock percentage weight by mineral phase) %						
Rock type	Proximity to fault (m)	Quartz	K-feldspar	Plagioclase	Anatase	Illite & Mica	Kaolinite	Illite & smectite
Unfaulted sandstone	100	84.6	3.3	–	0.7	6.0	5.4	–
Fractured sandstone	50	92.4	2.3	–	–	1.8	3.5	–
Fractured sandstone	30	89.7	4.0	–	–	2.2	4.0	–
Intensely fractured sandstone	5	90.4	4.6	–	–	1.8	3.2	–
Intensely fractured sandstone	3	78.2	4.3	–	0.6	7.6	9.3	0.2
Eumeralla formation sandstones		XRD analysis (whole rock percentage weight by mineral phase) %						
Rock type	Proximity to fault (m)	Quartz	K-feldspar	Plagioclase	Chlorite	Illite & Mica	Kaolinite	Illite & smectite
Unfaulted sandstone	225	38.9	7.1	32.3	6.7	14.6	-	0.5
Fractured sandstone	104	33.3	6.9	29.6	6.5	19.4	1.3	–
Fractured sandstone	64	42.0	7.4	28.8	6.2	12.5	3.1	–
Intensely fractured sandstone	13	38.9	5.6	23.2	5.5	22.7	4.1	–
Intensely fractured sandstone	0.5	40.1	7.3	27.4	5.6	14	5.3	0.3

Note. See Section 2.1 for method. XRD, X-ray diffraction.

Table 2
XRD Analysis of Clay Fraction Samples of Scapa and Eumeralla Sandstone to Determine Percentage Weight by Mineral Phase

Scapa sandstone			XRD analysis (clay fraction percentage weight by mineral phase) %				
Rock type	Proximity to fault (m)	Clay volume	Kaolinite	Illite	Illite& smectite	Quartz	Jarosite
Unfaulted sandstone	100	3.1	75.2	11.4	-	10.3	3.1
Fractured sandstone	50	2.3	80.5	7.7	-	11.9	-
Fractured sandstone	30	3	84.6	12	-	3.4	-
Intensely fractured sandstone	5	2.5	75.3	14.8	-	9.9	-
Intensely fractured sandstone	3	4.2	75.0	14.6	5.8	4.6	-
Eumeralla sandstone			XRD analysis (clay fraction percentage weight by mineral phase) %				
Rock type	Proximity to fault (m)	Clay volume	Kaolinite	Illite	Illite& smectite	Quartz	Chlorite
Unfaulted sandstone	225	5.8	-	6.9	9.0	1.2	82.8
Fractured sandstone	104	7.4	20.7	12.6	17.2	1.5	47.9
Fractured sandstone	64	9.1	27.1	28.7	-	2.4	41.7
Intensely fractured sandstone	13	7.2	24.3	19.8	-	2.3	53.7
Intensely fractured sandstone	0.5	4.3	37.5	15.2	7.2	2.7	37.4

Note. See Section 2.3 for method. XRD, X-ray diffraction.

and there is no change in the intensity/density of microfractures with proximity to the fault i.e., increased deformation (Supporting Information S1). SEM-CL images from some damage zone samples show healed/quartz cemented intergranular microfractures (Supporting Information S1), but it is assumed that most microfractured grains were subsequently cataclased and comminuted.

The Castle Cove Fault is also a basin-scale normal, reverse-reactivated fault (displacement >250 m, strike length ca. 30 km) located in the eastern Otway Basin (Australia) hosted in the Eumeralla Formation sandstone (Debenham et al., 2018). Eumeralla Formation sandstones were sampled from coastal cliff exposures at various distances (up to 225 m) from the fault surface. The Eumeralla sandstone is a fine- to medium-grained, compositionally immature volcaniclastic arenite deposited in a high energy, fluvial environment with braided channels, flood plains and shallow lacustrine deposits (Duddy, 2003; Krassay et al., 2004). Samples consist of moderately sorted sands with a modal grain diameter around 200 μm (Figure 4b). Mineralogy is dominated by quartz and plagioclase (albitic) feldspar with some K-feldspar, chlorite and mica grains (annotated in Figure 4b). Clay volume is 5.8% comprising chlorite and some illite and smectite (Table 2). Authigenic, pore-lining chlorite is uniformly distributed on pore walls, forming "internal shells" within pores up to 10 μm thick against the pore wall. The Eumeralla sandstone has a mean porosity of 17.3%. Pore size distributions show a visibly bimodal pattern of large intergranular pores (up to 500 μm diameter) with irregular perimeters and smaller intergranular pores encircled by pore lining chlorite. Extensive fine, intragranular microfractures are observed in unfaulted and faulted samples and contribute to a fraction of the porosity but show no common alignment and no change in the intensity/density of the microfractures with proximity to the fault (Figure 4b and Supporting Information S1) (Debenham et al., 2019).

A total of 137 core plugs (25.7 mm diameter x 60 mm length) were made from 27 sample blocks of the Scapa and Eumeralla sandstone. Cores were made from "damage zone" rocks only as the North Scapa Fault core was too brecciated to be cored and the Castle Cove Fault core is not exposed at the surface. Blocks were cored in three orientations relative to the fault plane: normal to the fault (x), along fault strike (y) and parallel to fault dip (z) (after Farrell et al., 2014). An appraisal of core plug quality was conducted and any cores with macroscopic structural features that may affect permeability (e.g., fractures or compaction bands) were removed. Core plugs were washed and dried for 24 h in an oven at 40°C to remove all pore water.

4. Results

Changes in microstructural properties of mineralogy, clay distribution and morphology and petrophysical properties of porosity, permeability and pore connectivity, were documented from faulted sandstones containing authigenic kaolinite and authigenic chlorite (respectively). These characteristics were interpreted through their location with respect to the fault surfaces, used here as a proxy for progressive fault-related deformation. Previous studies on the Scapa and Eumeralla sandstones have described the fault architecture and fault rock types identified in the North Scapa Fault and Castle Cove Fault zones (Debenham et al., 2018; Farrell & Healy, 2017). Fault rock types identified in these studies included, fault breccia, containing clasts of cataclasite in fine matrix; cataclasite, containing extensive microfractures, grain comminution and shear fractures; intensely fractured sandstone, containing a measured increased density of microfractures and intragranular and transgranular microfractures; fractured sandstones, containing moderate densities of macrofractures and some intragranular microfractures and some visible sedimentary lamination. Due to sampling limitations, blocks were only sampled from zones of fractured fault rock in the damage zone and cores were plugged carefully to avoid macro scale features that would dominate the hydraulic conductivity at a core plug scale. Zones demarcating these fault rock types vary between the different size faults, with fractured sandstones located up to 104 m from the Castle Cove fault and <50 m from the North Scapa fault. At Castle Cove the intensely fractured sandstones are located <14 m from the fault plane and <5 m at North Scapa.

4.1. Microstructural Observations

Kaolinite-bearing Scapa sandstones were sampled between 3–100 m from the North Scapa fault surface and chlorite-bearing Eumeralla sandstones were sampled between 0.5–225 m from the Castle Cove fault (Figures 5 and 6). Kaolinite was identified from SE images using spectral data produced from energy-dispersive X-ray analysis (EDS) which display equal height Si and Al peaks on EDS spectra, typical of kaolinite. Chlorite was identified from Si, Al, Mg and Fe peaks on EDS spectra. The mineral composition of SE imaged samples was quantified using X-ray diffraction (XRD) whole rock analysis (Table 1). Further details on XRD analysis available in Supporting Information S1.

4.1.1. Distribution of Authigenic Kaolinite in Scapa Sandstone

Samples of unfaulted Scapa sandstone sampled 100 m from the fault surface show a volumetric composition of 84.6% quartz grains with quartz cement overgrowths and 3.3% "blocky" euhedral K-feldspar grains (identified by Si, Al and K peaks on EDS spectrum) surrounded by authigenic K-feldspar overgrowths and 5.4% kaolinite clays (Figures 5a and Table 1). Kaolinite crystals are unevenly distributed and often formed in localized areas at the end of K-feldspar grains, normal to the plane of twinning. Fractured sandstone sampled 50 m from the fault plane also comprise quartz, K-feldspar and moderately less (3.5%) kaolinite (Figure 5b). Grain fractures are consistently observed in K-feldspars and many grains are considerably dissolved and appear as remnant 'nuggets' in the center of macropores (Figure 5b). In this example, lines of high relief are noted as preferentially dissolved–or 'picked out' – cleavage planes along the grain (Figure 5b). Throughout the sample, characteristic 'books' of stacked kaolinite crystals are observed coating the perimeter of macropores. These clay aggregates are moderately packed with crystal faces showing no preferred orientations and visible microporosity between packages. Fractured sandstones 30 m from the fault surface samples comprise quartz, K-feldspar and slightly more (4%) kaolinite (Figure 5c). In these samples, large secondary pores (>100 μm) formed by complete dissolution of K-feldspar are observed as large 'empty nests' lined by evenly distributed, well-developed kaolinite crystals. Transgranular fractures are also observed in BSE (back-scattered electron) images, however these pores do not contain authigenic clays indicating that precipitation of kaolinite was pre- and/or syn-faulting (Farrell & Healy, 2017). Intensely fractured sandstones sampled 5 m from the fault surface comprise quartz, K-feldspars (present as fractured, cataclased and partially dissolved grains) and slightly less (3.2%) kaolinite (Figure 5d). Pore fabric includes some partially clay-filled and some completely occluded macropores. In clay-filled pores, kaolinite aggregates are densely packed and compressed against framework grains. At these magnifications, micropores within clays are not visible. Intensely fractured sandstones sampled 3 m from the fault surface comprise quartz, K-feldspar and greatly increased (9.3%) kaolinite (Figures 5e and Table 1). Intergranular pores are often completely

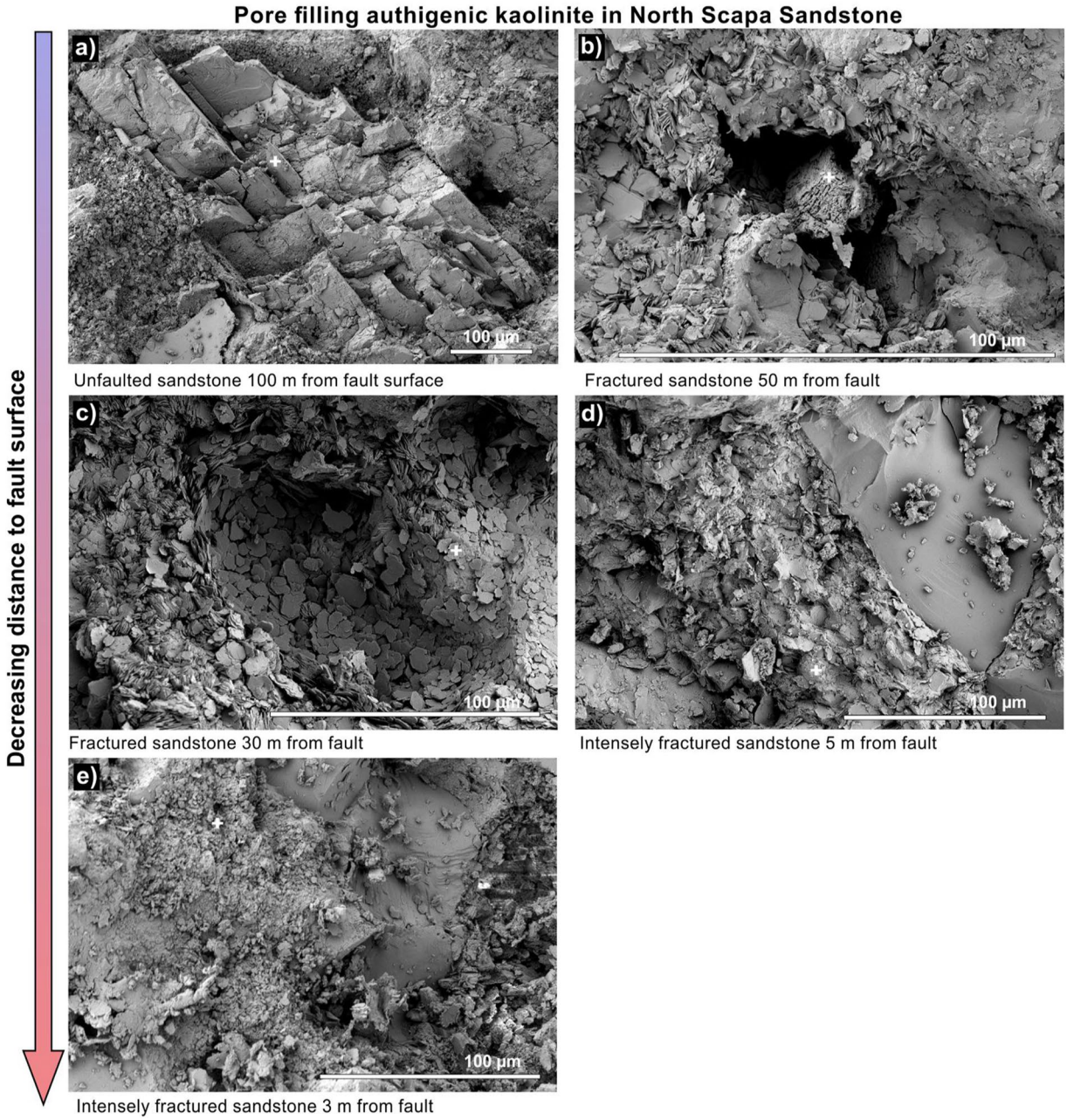

Figure 5. Secondary electron micrographs showing deformation and dissolution of K-feldspar grains and reprecipitation as kaolinite clays with decreasing distance to North Scapa fault surface. (a) Micrographs show, and (b) K-feldspar grains in the unfaulted rock (100 m from the fault surface) that have been fractured and dissolved. (c) Secondary kaolinite clays that have been precipitated within secondary pore space remaining from the original grain. (d) Increased deformation of kaolinite clays via compaction and shearing in samples located 5 m from the fault surface. (e) Grain comminution and chaotic distribution of clays 3 m from the fault surface. Corresponding mineral compositions (from X-ray diffraction whole rock analysis) show limited change in mineral proportions (See Table 1).

occluded by authigenic clays that present as a fine-grained semi-homogenous 'paste' with no discernible organisation at this scale.

4.1.2. Distribution of Authigenic Chlorite in Eumeralla Sandstone

Microstructural examination of Eumeralla sandstones identified authigenic chlorite clays in all samples in different amounts and with a variety of distribution styles. Unfaulted sandstones sampled 225 m from the fault surface show chlorite clays filling many intergranular macropores (Figure 6a). The chlorite volume

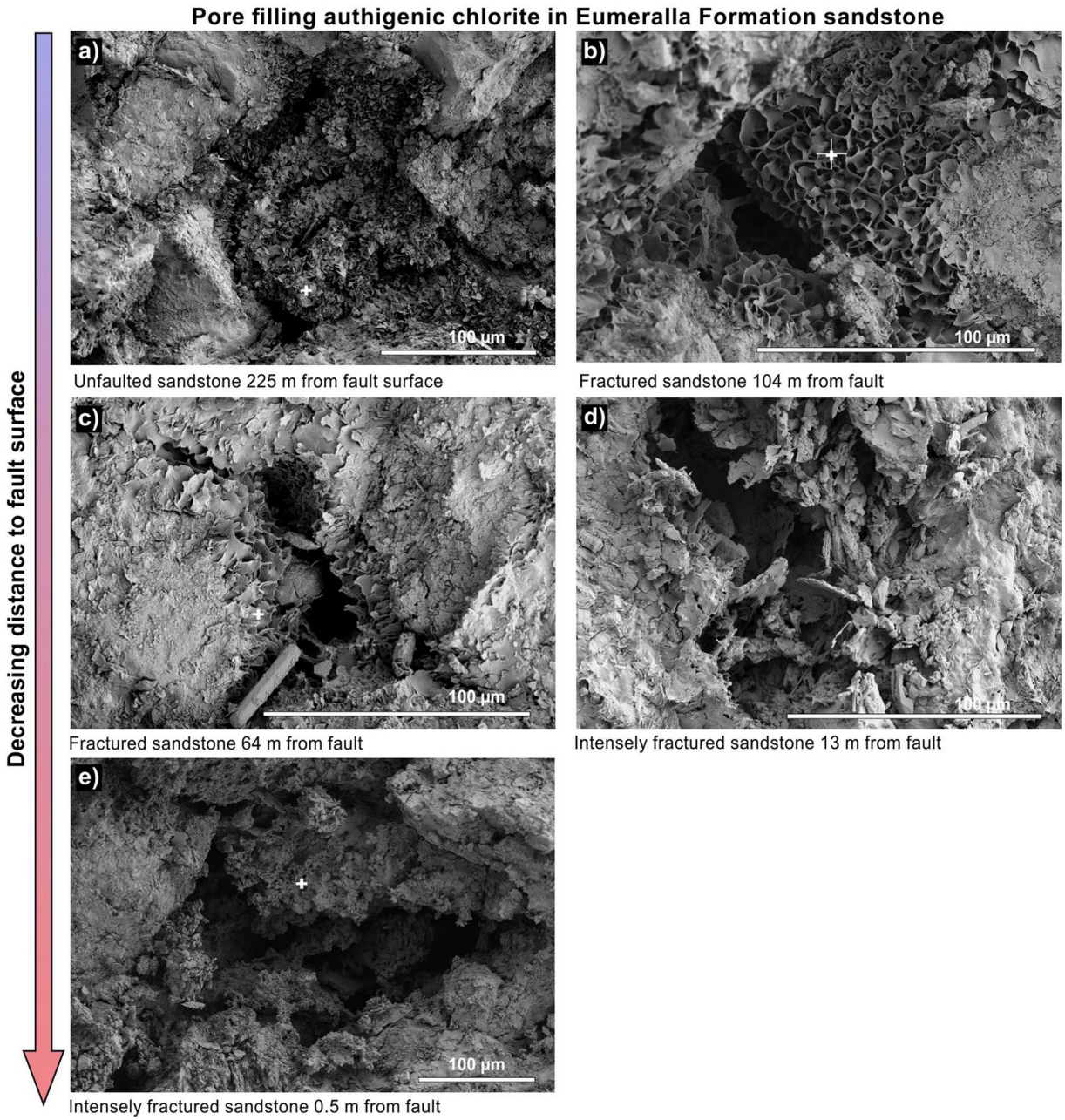

Figure 6. Secondary electron micrographs showing deformation and changing distribution of authigenic chlorites with decreasing distance to Castle Cove Fault surface. Micrographs show (a) Euhedral pore lining and pore-filling "garlands" of chlorite changing to, (b and c) solely pore lining clays and (e) to clumps of small poorly formed crystals with rough textures. Corresponding mineral compositions (X-ray diffraction data) show limited change in chlorite content between samples but show inclusion of kaolinite with decreasing distance to the fault (see Table 1).

was 6.7%. Chlorite lines the edges of pores with individual crystals oriented with faces perpendicular to the framework grains and thick garlands of packed chlorite crystals coiled in the center of macropores (Figure 6a). Chlorite garlands are not present in fractured sandstones sampled 104 m from the fault surface; however pore lining chlorite remains coherent (Figure 6b). Individual crystal faces are apparent, but the crystal edges appear to have coalesced and formed continuous rims surrounding a web of 5–10 µm micropores (Figure 6b). Pore lining chlorite is maintained in fractured sandstones sampled 64 m from the fault surface (Figure 6c). However, the density of individual crystals making up the lining is lower, and clays exhibited a flattened, scaly texture lacking the geometric crystal arrangements observed in pore lining

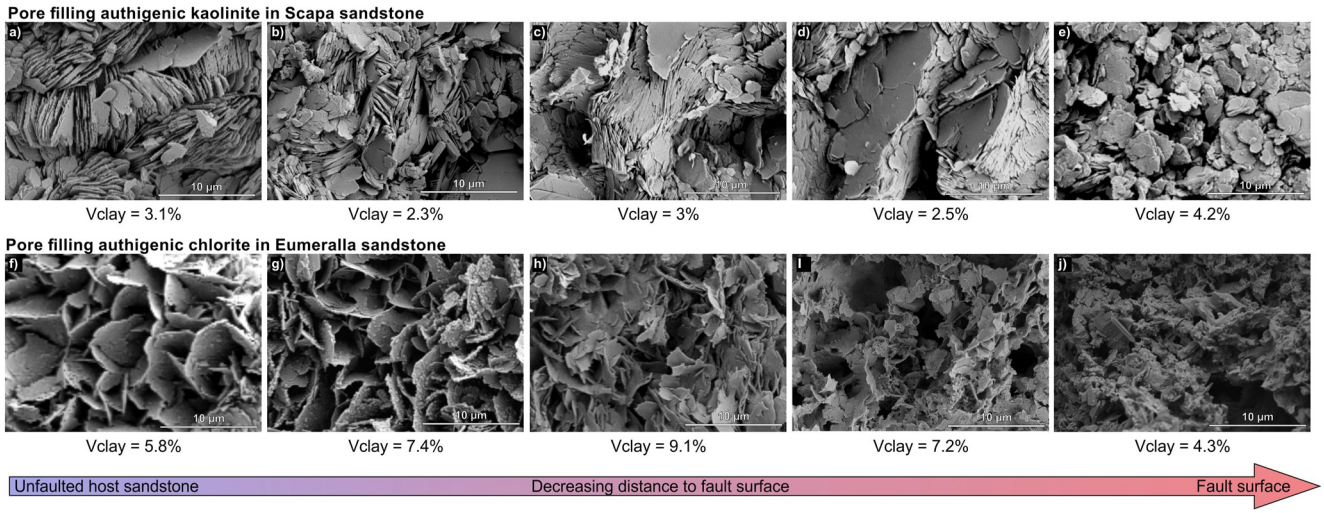

Figure 7. High magnification secondary electron images showing morphologies of authigenic clays in sandstones located at varying distances from fault surfaces. Micrographs (a–e) show progressive compaction and eventual comminution of kaolinite grains in the Scapa sandstone from (a) well crystallized large crystals (5–10 μm) stacked in large vermiforms in unfaulted sandstones through (c) tightly packed and compressed "books" of crystals showing preferential alignment and low shear to, (e) small (<5 μm) disaggregated individual kaolinite crystals with ragged edges. Micrographs (f–j) show progressive reduction in chlorite crystal diameter in the Eumeralla sandstone from (f and g) well-formed euhedral "rosettes"; typical of authigenic chlorite to, (h and i) deformed and compacted crystals to, (j) fine crystal mesh.

chlorite identified further away from the fault surface. Intensely fractured samples 13 m from the fault surface contain larger intergranular macropores as much of the euhedral, pore lining clays has been replaced by altered, jagged, irregular 'flakes' of authigenic chlorite and smaller individual 'books' of kaolinite that partially fill pores (Figure 6d). In these samples, chlorite volume is slightly lower (5.5%) and discernible plate like chlorite crystals (around 10 μm diameter) appear 'shredded' (containing many holes). Intensely fractured sandstones sampled 0.5 m from the fault surface contain 5.6% chlorite volume (Figures 6e and Table 1). Macropores are open and partially filled with chlorite clays that have a rough texture composed of a fine aggregate of crushed and/or cataclased crystals. Within clays micropores are common (Figure 6d).

4.1.3. Effect of Faulting on Clay Morphologies

We investigated the changing morphology and texture of clay particles using high magnification SE images. In unfaulted Scapa sandstones kaolinite formed as well-crystallized, large (10 μm) pseudohexagonal plates (Figure 7a). Crystals are stacked with faces parallel to each other in a book morphology typical of kaolinite. These books are generally ~10 μm thick with some aggregates of clay crystals termed vermiforms measuring over 30 μm. Within localized domains of kaolinite located in macropores, crystal faces and books are moderately aligned forming compact textures with no discernible microporosity. Fractured sandstones 50 m from the fault surface also contain authigenic kaolinite with a distinctive book morphology, however books are generally <5 μm thick (Figure 7b). Here, crystal faces display a broader range of alignments forming a more dispersed fabric with visible micropores between crystals. In intensely fractured sandstones 5 m from the fault surface kaolinite "books" are tightly packed showing preferred alignment of multiple stacks (Figure 7c). Compared to the vermiform morphologies observed in unfaulted samples, the ends of kaolinite crystals within books are staggered and skewed by small amount of shearing analogous to a sliding deck of cards. Additional images from the same sample show the exposed top surfaces of these decks of sheared crystals and reveal elongate exposed surfaces between these assemblages (Figure 7d). High magnification images from cataclased sandstones 3 m from the fault surface feature a majority of smaller (<5 μm) crystals of kaolinite with rounded shapes and ragged edges (Figure 7e). In these samples books of kaolinite have either never been formed or have been disassembled, breaking down aggregates into individual crystals, which were then further comminuted into smaller poorly crystallized grains. Corresponding XRD data (Table 2) presents the mineralogical make-up of sample clay volume (all grains <2 μm). Volumes of clay from kaolinite bearing sandstones are quite consistent, between 2.3% from unfaulted rocks to 3.1% at 5 m from the fault surface (Table 2 corresponding to Figures 7a–7d). Samples 3 m from the fault contain slightly

higher clay volume of 4.2% (Table 2 corresponding to Figure 7e). Clay volumes consistently comprise at least 75% kaolinite in all samples.

In unfaulted Eumeralla sandstones chlorite lies in clusters of plate-like, pseudohexagonal crystals with rounded edges arranged in a "rosette" pattern typical of authigenic chlorite (Figure 7f). In these samples, crystals sizes range from 5–10 μm in diameter and <0.5 μm thick. Samples collected from 104 m from the fault surface reveal the onset of fault deformation as a disruption of the regular chlorite "rosettes" caused by compaction, however individual chlorite crystals remain between 5–10 μm diameters and maintain the typical pseudohexagonal morphology (Figure 7g). Chlorite crystals in deformed sandstones 64 m from the fault surface exhibit a platelet morphology seen in unfaulted clays but with frayed, cuspate edges and a slightly smaller diameter (3–8 μm) (Figure 7h). Crystal arrangements are irregular with varied packing density, from tightly packed on the right of the image to loosely packed and porous in the center. Some crystals are aligned parallel to each other possible due to fault related shearing. Samples collected 13 m from the fault surface comprise chlorite clays with flake like texture of small (1–5 μm) crystals with ragged edges and pitted faces. Other flattened crystals are observed forming a "mat like" texture with bimodal micropore spaces of 1 and 5 μm diameters (Figure 7i). Typical chlorite morphology is not helpful in identifying cataclased chlorite in sandstones sampled 0.5 m from the fault surface and identification was only possible through EDS analysis. In these samples, chlorite clays are present as fine-grained (<3 μm) crushed crystals with angular edges and a blocky morphology. The overall texture of these chlorites is rough but regular (Figure 7j). Corresponding clay fraction analysis shows an increase in the volume of clay from 5.8% in unfaulted samples to 9.1% at 60 m from the fault surface (Table 2). Clay volume decreases to 7.2% 13 m from the fault and 4.3% at the fault surface (Table 2 data corresponding to Figures 7i and 7j respectively). Unfaulted rock clay volumes are dominated by authigenic chlorites (Figure 7f) which generally decreases to < 50% in faulted samples (Figures 7g–7j). This decrease in chlorite clays was accompanied by a progressive increase in kaolinite from 20.7% 161 m from the fault surface to 37.5% at the fault surface (Table 2). Kaolinite grains are not observed in the SE images from the fault surface, but illite laths associated with chlorite are present.

4.2. Petrophysical Properties

Measurements of permeability, porosity and pore connectivity for the two sandstones are shown in Figures 8–11. Permeabilities measured on 59 core plugs of kaolinite-filled Scapa sandstone show a range in the magnitude of permeabilities from 7.89×10^{-18} m^2 to 2.9×10^{-14} m^2 with no overall trend relating to fault surface proximity (Figure 8). Results are graphed by fault rock type including: (a) unfaulted sandstones (>100 m from the fault); (b) fractured sandstones (between 50 and 30 m); (c) fractured sandstone with secondary dissolution pores (between 30 and 10 m); and (d) intensely fractured sandstones (<10 m from fault surface). Anisotropy of permeability is noted in both unfaulted sandstones and intensely fractured sandstones <10 m from the fault plane (Figures 8a and 8d respectively). However, while the orientation of maximum fluid-flow (k_{max}) in unfaulted samples with visible sedimentary bedding planes is parallel to fault strike, k_{max} in faulted samples containing compacted and sheared kaolinite "books" is down fault dip (Figure 8d). Moderate mean porosities (11.8%) and low mean permeabilities (1.86×10^{-16} m^2) measured from unfaulted sandstones (Figure 8a) decrease to 10.2% and 2.96×10^{-17} m^2 with the onset of fault deformation in fractured sandstones (Figure 8b). Fractured sandstones containing substantial secondary dissolution pores demonstrate relatively broad petrophysical ranges with porosities ranging over 5% and an increased mean porosity of 12.6% and permeabilities ranging over four orders of magnitude and an increase in mean permeability to 6.9×10^{-16} m^2 (Figure 8c). Mean porosities and permeabilities of intensely fractured and cataclased sandstones are reduced to 8.9% and 1.48×10^{-16} m^2 (akin to mean permeabilities of unfaulted sandstones) (Figure 8d).

In comparison, permeabilities measured from 78 chlorite-filled Eumeralla sandstone core plugs show a distinct trend of increased permeabilities with decreased distance to the fault surface with permeabilities ranging from 9.87×10^{-18} m^2 to 2.7×10^{-15} m^2 (Figure 9). Porosity also increases from 16.8% mean porosity in unfaulted sandstones containing both pore lining and pore occluding authigenic chlorite (Figures 9a) to 23.3% in fractured sandstones containing only pore lining chlorite (Figure 9b). However, while mean permeabilities continue an upward trend in intensely fractured sandstones with pores containing cataclased chlorite, mean porosities in these samples barely change at 22.8% (Figure 9c).

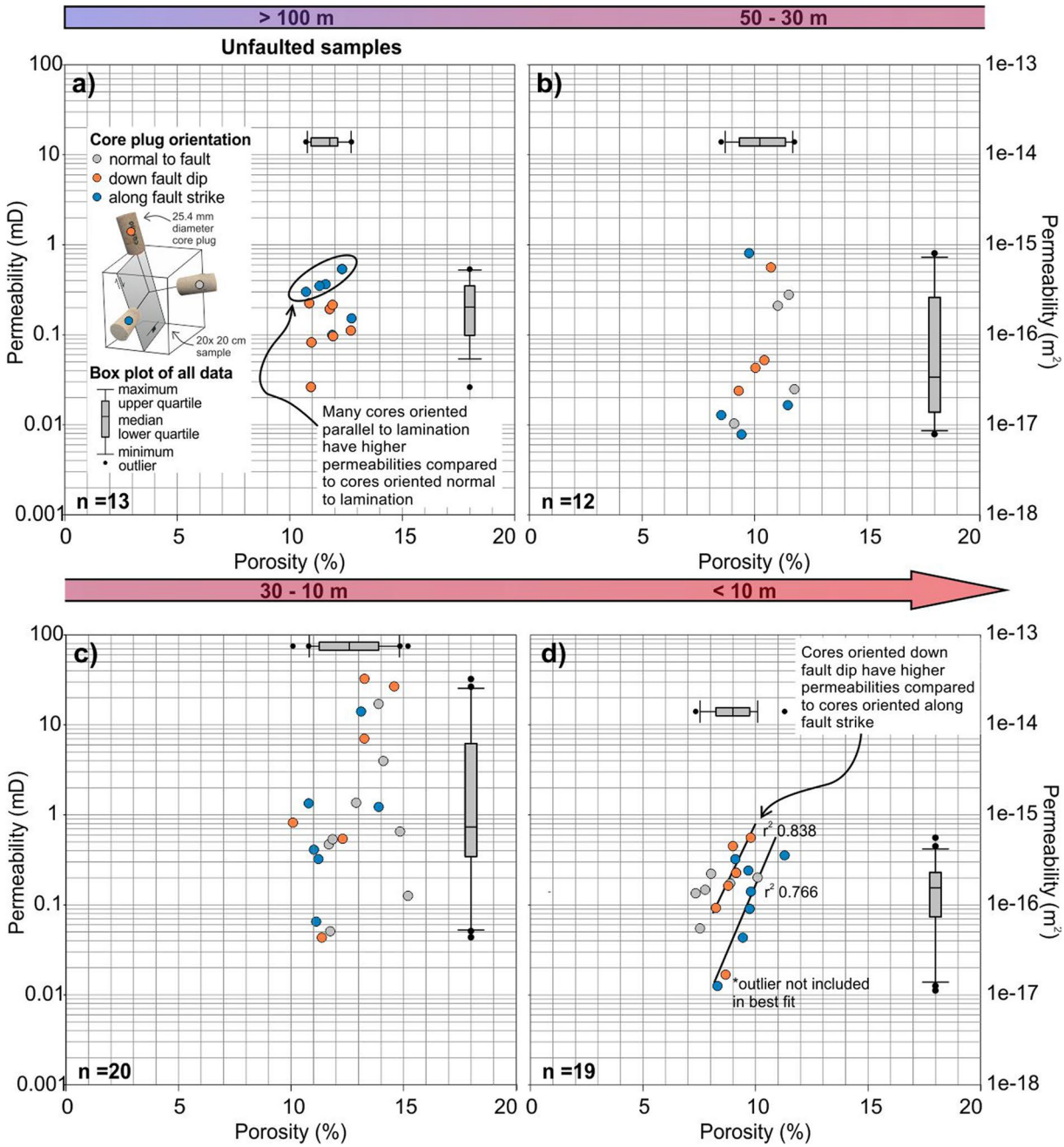

Figure 8. Porosities and permeabilities of North Scapa Sandstone sampled at a range of distances to a fault surface. Gray box plots show the statistical ranges in porosity and permeability data including the mean values and interquartile ranges. Linear regression lines are plotted to highlight data trends. (a–c) Overall results show an increase in permeability from unfaulted sandstone to fractured sandstone sampled 30–11 m from the fault surface. However, neither permeability or porosity show an overall trend corresponding to sample location and permeabilities of samples <10 m from the fault surface (d) are nearly identical to unfaulted sample permeabilities (a), albeit with lower porosities. (d) Development of anisotropic permeability is noted in samples taken <10 m from the fault surface with maximum permeability in core plugs oriented down fault dip.

4.3. Capillary Properties

Mercury injection porosimetry (MIP) was conducted on samples to investigate the dependence of quantified petrophysical properties on the observed pore microstructures of different samples. Mercury threshold pressure curves drawn from MIP data are useful to (a) to assess the connectivity of the pore types identified from microstructural observations, using the shapes of curves (Thomeer, 1960) and (b) consider the

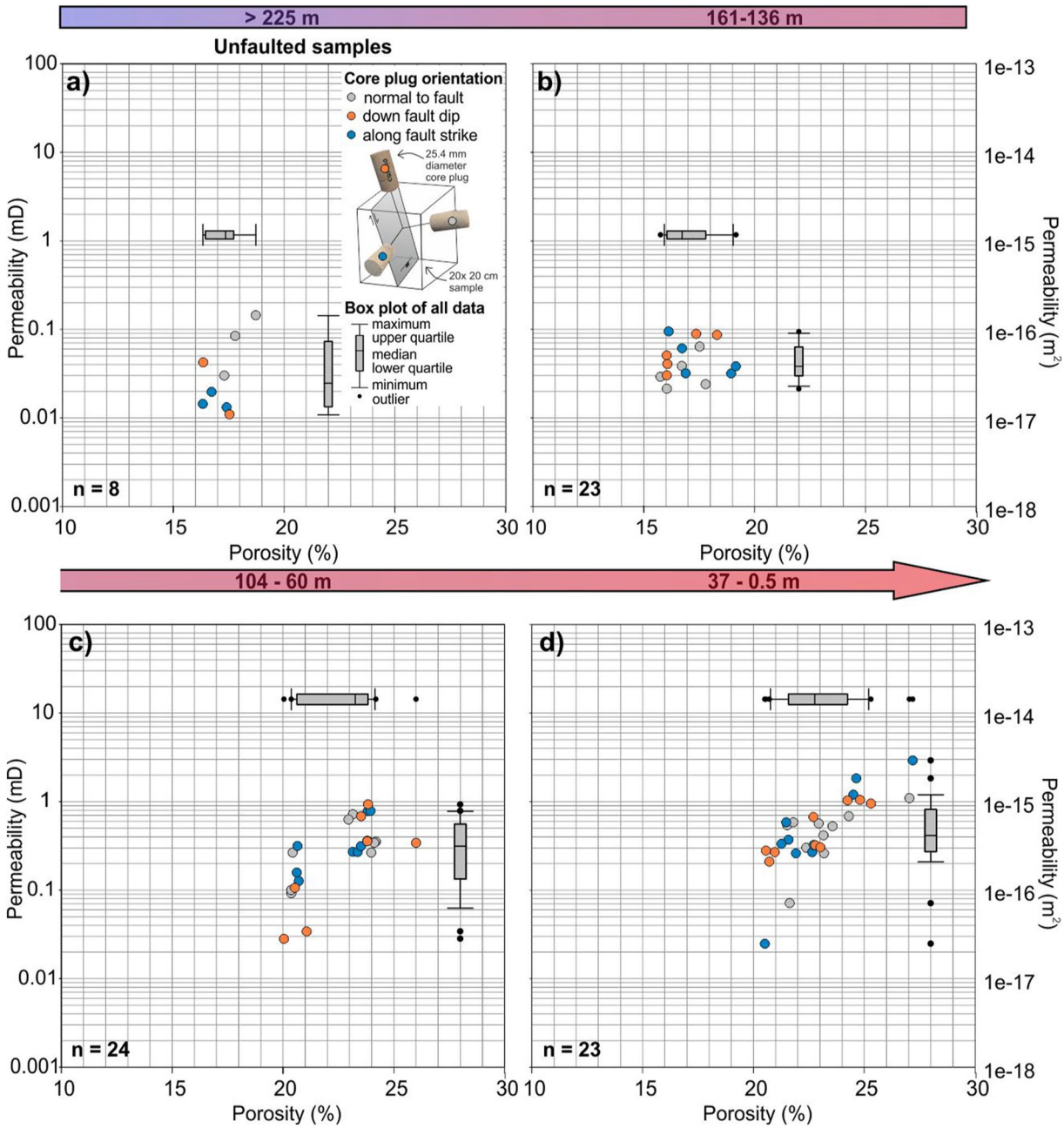

Figure 9. Porosity and permeability of Eumeralla sandstone sampled at a range of distances from a fault surface. Gray box plots show the statistical ranges in porosity and permeability data including the mean values and interquartile ranges. (b and c) Progressive increase in permeability and porosity with mean permeability increasing by one order of magnitude from 2.96×10^{-17} m^2 to 2.96×10^{-16} m^2 between 104 and 161 m from the fault surface. (b and d) Porosity also increases from ~16% to 22%.

contribution of these pore networks to measured permeabilities, using the parameters of curves, including displacement pressures and capillary threshold pressures also known as "apex" pressures. Here, displacement pressure describes the minimum pressure needed to form a continuous filament of mercury through the sample (Schowalter, 1979) while the capillary threshold pressure/"apex" pressure describes the inflection from decreasing gradient to increasing gradient at which point it is assumed that the dominant pore networks controlling permeability have been saturated (Swanson, 1981).

Mercury injection pressures were measured from seven unfaulted and faulted samples of kaolinite filled Scapa sandstone (Figure 10a). Samples furthest from the fault surface (100 and 50 m) exhibit a moderate

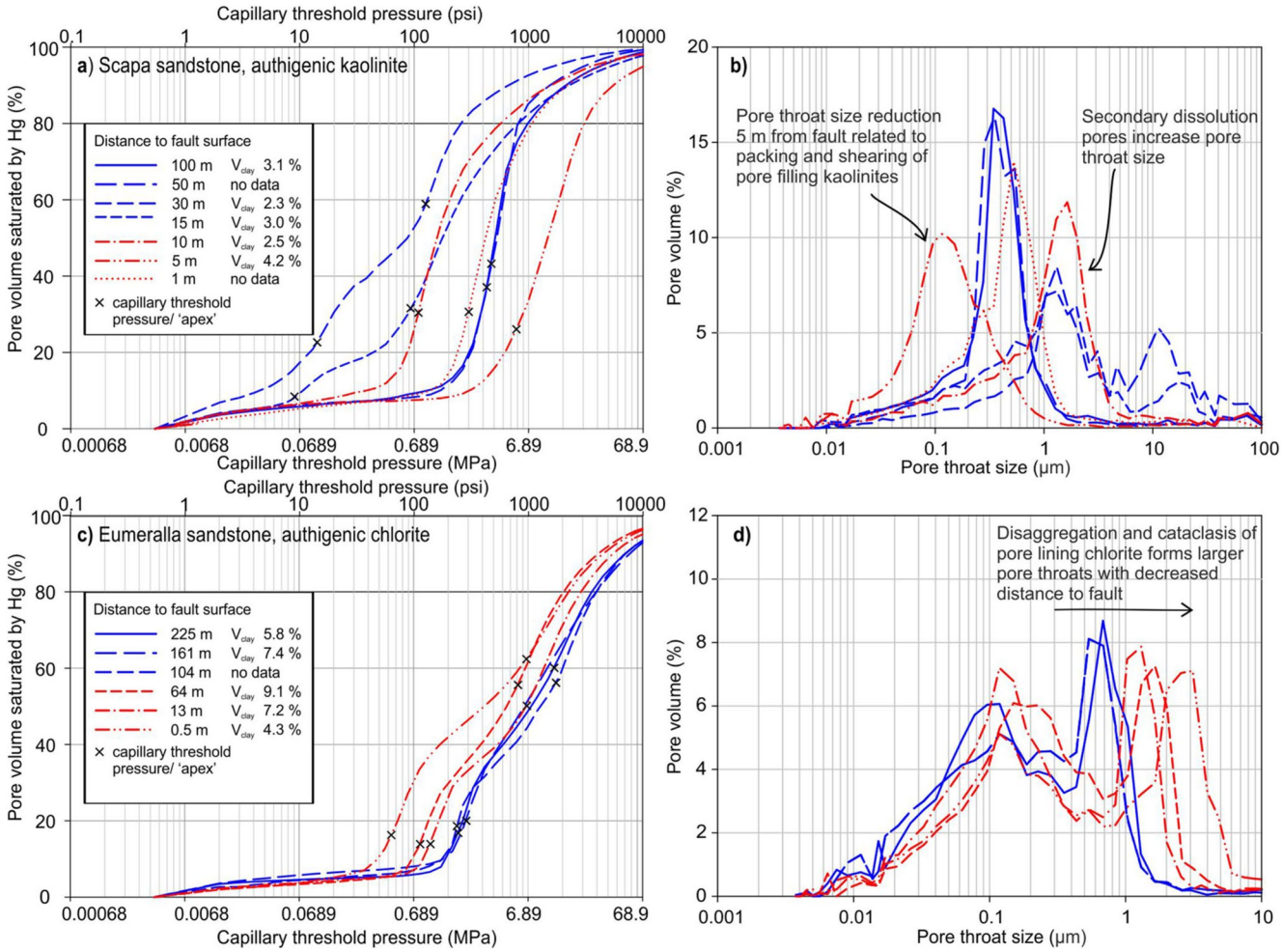

Figure 10. Mercury injection capillary pressure curves for samples of sandstones containing authigenic kaolinite and authigenic chlorite collected from a range of distances from a fault surface. (a) Kaolinite filled Scapa sandstones show variable saturation pressures with no clear correlation to sample location. In contrast, (c) shows that the pressure required to saturate chlorite filled Eumeralla sandstones decreases with increasing proximity to the fault surface. Corresponding graphs show pore throat size distributions and incremental pore volume derived from Mercury injection porosimetry data for (b) kaolinite filled Scapa sandstones and (d) chlorite filled Eumeralla sandstones.

initial displacement pressure (~1.4 MPa) followed by a steep slope then a moderate gradient plateau around 85% Hg saturation. This curve shape indicates that the connected pore network is dominated by macropore with a homogenous pore throat size distribution around 0.3 μm (Figure 10b). At 30 and 15 m from the fault surface, initial displacement pressures decrease substantially to <0.0689 MPa and mercury pressure curves are both defined by moderate gradient slopes with two distinct inflection points termed "double curves" (Thomeer, 1960). The limited variation in gradient between the slope and short plateaus suggests a broad distribution of pore throat sizes, whereas the "double curve" characteristic reveals two discrete pore networks with different capillary entry pressures dominated by two sets of macropores with modal pore throat sizes <1 μm and >10 μm respectively (Figure 10b). Close to the fault surface (10 and 5 m) samples show significantly varied displacement pressures from ~0.4 MPa, 10 m to the fault increasing to >2.75 MPa, 5 m from the fault (Figure 10a). Both curves show slopes with steep gradients reflecting homogeneous pore throat size distributions of >1 and 0.1 μm respectively (Figure 10b). One meter from the fault surface displacement pressures are ~1.37 MPa akin to pressures from unfaulted samples. Remarkably, the pore network quantified in these most faulted samples is also dominated by a homogenous network of pores with throats sizes ~0.5 μm.

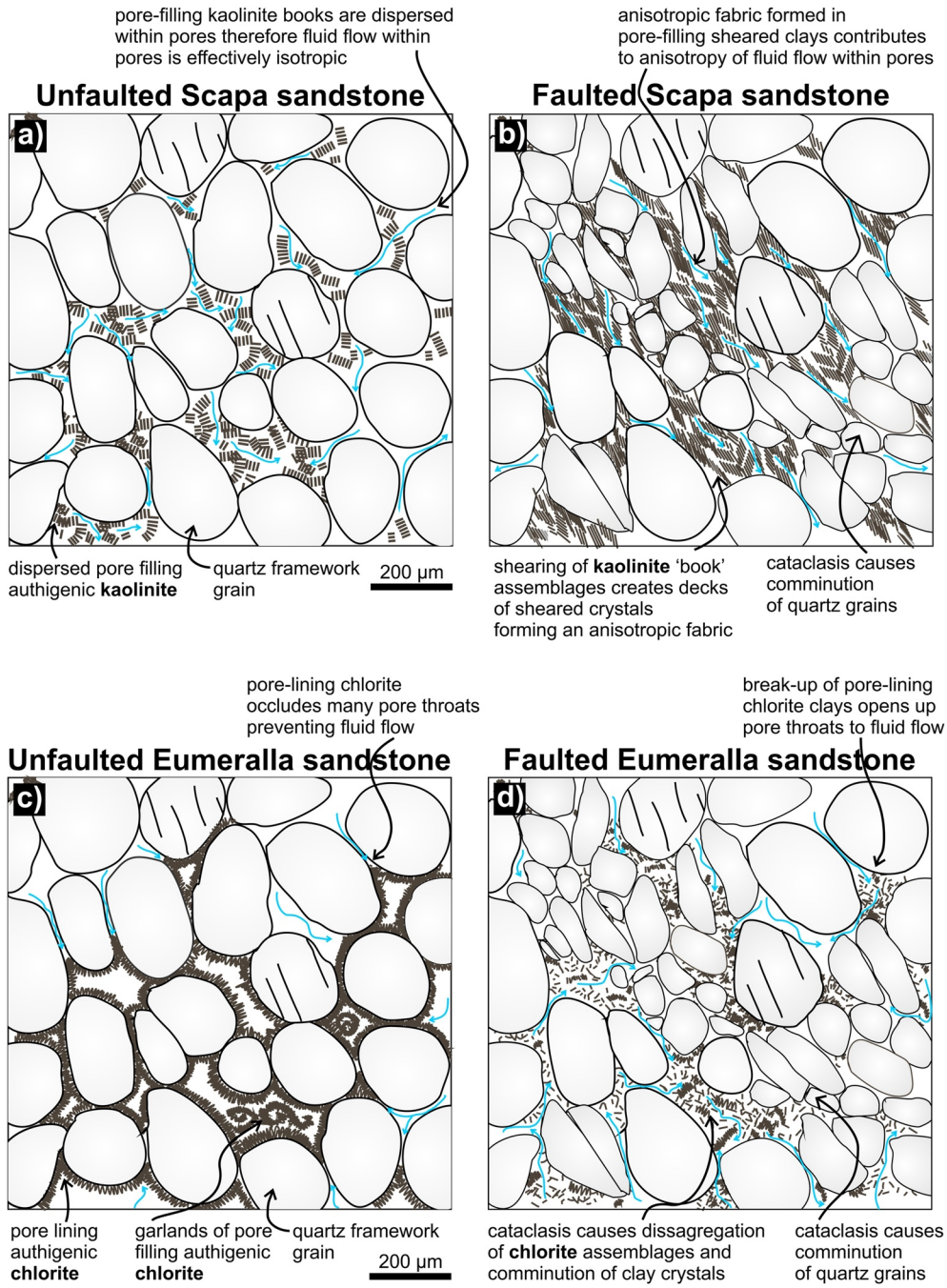

Figure 11. Diagrams showing how faulting of phyllosilicate rich sandstone containing authigenic chlorite and kaolinite changes the rock microstructure and influences fluid-flow within pores and pore throats. Features on sketches were collated from a number of back-scattered electron microscope images presented in Supporting Information S1. (a) Authigenic kaolinite present as dispersed vermiforms within pores creates limited obstruction to fluid-flow. (b) In contrast, fracturing and shearing of quartz grains and shearing of kaolinite books can channel fluid-flow. (c) Pore lining authigenic chlorite reduces pore surface area, blocking pore throats and limiting fluid-flow. (d) In contrast, cataclasis via fault deformation causes grain comminution of both quartz framework grains and pore lining chlorite opening up pore throats to fluid-flow, thereby increasing permeability.

In comparison, faulted samples of chlorite-filled Eumeralla sandstones show a distinct correlation between decreasing distance to the fault surface and decreasing displacement pressures (Figure 10c). An unfaulted sample and faulted samples furthest from the fault surface (225 m, 161 and 104 m) all have initial displacement pressures around 1.37 MPa (comparable to displacement pressures of unfaulted Scapa sandstone). Closer to the fault surface displacement pressures of faulted samples decrease from ~0.68 MPa to <0.34 MPa. Mercury threshold pressure data from Eumeralla sandstone samples all present as "double curves" as the overall gradient of the curve decreases in samples closer to the fault surface. Points of inflection between the curve plateaus and slopes becomes more pronounced in samples collected <13 m from the fault surface (Figure 10c). The double shape of Eumeralla sandstone mercury threshold curves is reflected in bimodal peaks on the incremental pore volume plots (Figure 10d). These plots mainly show a continuous range of pore throat sizes with bimodal peaks between 0.1 μm and <1 μm in samples over 100 m from the fault, and 0.1 μm and >1 μm in samples under 64 m from the fault surface (Figure 10d).

Capillary threshold pressures are calculated using the inflection point of mercury threshold curves (marked as black crosses on Figures 10a and 10c), described using a polynomial fit calculated using a bespoke MATLAB program (Open source code available at https://github.com/DaveHealy-github/micpThreshold). Two points of inflection are identified on Eumeralla sandstone curves depicting the parameters of the two dominant pore networks (Figure 10d). Primary capillary threshold values are regularly lower in samples <64 m from the fault plane at ~0.68 MPa compared to less faulted samples >104 m from the fault plane at ~1.72 MPa. Secondary capillary threshold pressures are also lower in samples closer to the fault plane ~6.89 MPa compared to less faulted samples at ~11 MPa (Figure 10c). In comparison, curves from most Scapa sandstones have a single point of inflection deriving capillary threshold pressures between 0.68 and 5.52 MPa with no correlation to distance to the fault surface (Figure 10a). Lower threshold pressures derived from samples located between 30 and 10 m from the fault are related to large secondary pores identified in the pore microstructure of these samples (Figure 10b).

5. Discussion

Our microstructural characterization of faulted sandstones containing authigenic kaolinite and authigenic chlorite has revealed previously unreported tectonic shearing and cataclasis effects on pore-residing, authigenic clay distribution and properties. Laboratory-based petrophysical measurements show a correlation between: (a) grain comminution and disaggregation of pore lining chlorite and increasing permeability; and (b) shearing of kaolinite "books" that create clay fabrics commonly aligned with k_{max} in rocks showing anisotropy of permeability. These changes in microstructural and petrophysical properties are related to the deformation mechanisms, and localisation of deformation is considered in the context of proximity to the fault surface and the original host rock structure. By interpreting these properties in a spatial framework around the fault and in the context of the sandstone facies, we can now discuss how these results relate to our current understanding of fault seal development in impure sandstones and how these results could be used to infer pore fabric patterns around other sandstone-hosted faults.

5.1. Impact of Faulted Authigenic Clays on Fluid-Flow and Capillary Threshold Pressure

In detail, permeability is principally a function of pore throat size (the narrowest aperture of a pore) and the tortuosity of the flow path. In low porosity rocks (i.e., crystalline granite), fault induced 'pores' and "pore throats" are produced by microfracturing and grain boundary cracking and these microstructures tend to form the main flow paths and dominate permeability. Increased bulk rock microfracturing, that is, closer to the fault surface, increases permeability in these zones (Evans et al., 1997). In contrast, fault-generated microfracture "pores" and "pore throats" in high porosity rocks (i.e., granular, porous sandstone) contribute little to the already large pre-existing porosity and their impact on the magnitude of permeability is smaller than in low porosity rocks. In addition, the common deformation mechanism of cataclasis in these rocks means that most fractured grains are comminuted into smaller angular fragments (Fowles & Burley, 1994) which are then compacted and can reduce permeability closer to the fault surface (Antonellini & Aydin, 1994). As shown in Section 2.1, BSE images from samples of unfaulted and faulted Scapa and Eumeralla Sandstones showed few intergranular fractures at all proximities to the fault surfaces (Supporting Information S1). The highest density of microfractures is in the unfaulted Eumeralla sandstone sampled

22 m from the fault. SEM-CL images of faulted Scapa sandstones reveal some filled microfractures in feldspars and some quartz but the deformation is accommodated by grain rearrangement and comminution via cataclasis and grain crushing, with few oriented intergranular fractures (Supporting Information S1). In porous, granular rocks, pore throats and flow paths are primarily controlled by grain size, grain packing structure and depositional and diagenetic mineralogy. Small amounts of authigenic clays have a significant role on controlling fluid-flow in unfaulted rocks (Wilson et al., 2014), where the physical constraint is constriction of pore throats rather than a decrease in pore diameter (Howard, 1992).

Microstructural results from this study have shown that: (a) Clay assemblages typical of both kaolinite and chlorite have been progressively deformed and disaggregated with decreasing distance to the fault surfaces in both the Scapa sandstone and the Eumeralla sandstone; and (b) crystal diameters of both authigenic kaolinite and authigenic chlorite crystals have been reduced close the fault surfaces (Figure 7). Relationships observed between diagenetic clays and tectonic fractures indicate that precipitation of clays occurred pre- and syn-deformation, as clays were not present in large transgranular fractures observed in BSE images (Debenham et al., 2019; Farrell & Healy, 2017) and–in the case of kaolinite precipitation–were related to fracturing and dissolution of K-feldspar. Based on this deformation history, crystal size reduction is interpreted as being caused by comminution via cataclasis or crushing rather than nucleation of smaller, poorly crystallized grains in previously faulted rocks. However, there is no obvious translation of crystal fragments–commonly associated with cataclasis–at the length scales we have analyzed, therefore fault deformed clays would need to be investigated at a higher magnification to validate this interpretation.

Preceding work on fault deformed Scapa sandstones showed how preferential deformation of weaker K-feldspar framework grains could form elongate grains with preferential alignment in the direction of shear which, when dissolved, left anisotropic pore fabrics and produced anisotropic permeability pathways (Farrell & Healy, 2017). Further analysis of these samples at a higher magnification has shown that these same deformation mechanisms have also produced anisotropic fabrics in pore-filling kaolinite (Figure 7d). Here, commonly oriented faces of compacted and sheared kaolinite "books" form anisotropic flow pathways within pores which likely *contribute* to the anisotropic permeability quantified from samples adjacent to the fault (Figure 11). Neither chlorite nor kaolinite (or illite) are swelling clays, therefore although using liquid permeants may alter measured permeabilities, the relative values and patterns of fluid-flow are likely to be consistent irrespective of the pore fluid used.

The Eumeralla Formation sandstone is noted for its thick pore-lining authigenic chlorite (Debenham et al., 2019; Duddy, 2003) which constricts/narrows pore throats and, even in this high porosity sandstone, greatly limits the magnitude of permeability. This study has also shown how fault deformation of authigenic chlorite has altered the distribution of aggregate forms by destroying pore residing chlorite garlands and disaggregating euhedral rosettes of pore lining chlorite (Figure 7). Destruction of chlorite clays has increased the porosity of faulted sandstones from mean porosities of 17% in unfaulted samples (located >225 m from the fault plane) to 23% in faulted samples (located <40 m from the fault plane) (Figure 9) and increased modal pore throat sizes (Figure 10d). This increase in porosity, combined with widening of pore throats, is likely to control the increased permeability measured in faulted samples (Figure 11). Grain size distributions were quantified for Eumeralla sandstones using laser particle analysis. Results showed a weak to moderate linear relationship of reducing grain size with increasing proximity to the fault surface (Section 4.5. and Figure 8 of Debenham et al., 2019). Smaller grains would be packed more tightly and decrease pore throat sizes so would not explain the observed patterns of increasing pore throat sizes with increasing proximity to the fault surface.

Mean permeabilities and capillary threshold pressures of faulted Scapa and Eumeralla sandstone were plotted alongside published petrophysical properties from unfaulted sandstones containing authigenic kaolinite and chlorite (Figure 12). While properties of faulted Eumeralla sandstone demonstrate a direct fit with published data from unfaulted chlorite-filled sandstones, faulted Scapa sandstone dominantly plots in two threshold pressure groups between 0.068 and 0.68 MPa and between 2.75 and 5.52 MPa corresponding to permeabilities ranging over an order of magnitude (Figure 12). Permeability data cross-plotted against capillary threshold pressure measurements also display a second group of higher threshold pressures ~6.89 MPa in the Eumeralla sandstone. These pores are identified as secondary inflection points on the mercury threshold curves (Figure 10c). In the case of curves with dual inflection points, physical properties

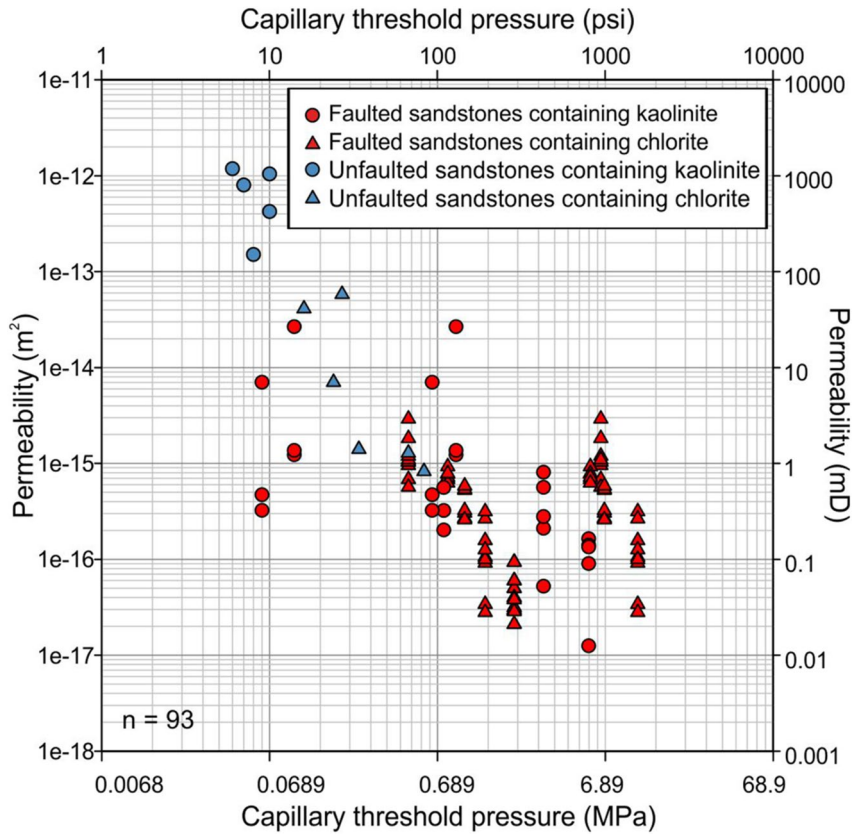

Figure 12. Capillary threshold pressures and mean permeabilities from faulted and unfaulted sandstones (averaged from the permeabilities of all core plugs made from a single sample) containing authigenic kaolinite and authigenic chlorite from this study (red) and unfaulted sandstones (blue) (after Neasham, 1977).

of fluid-flow are considered to be dependent on the parameters of the lower pressure inflections i.e., microstructural groups with larger pore throats.

5.2. How Faulted Authigenic Clay Morphologies Could Affect Reservoir Properties

Precipitation of authigenic clays is understood to reduce pore connectivity by constricting pore throats thereby reducing conductivity (Wilson et al., 2014). However, results from this study have shown that cataclasis of authigenic chlorite in fault zones can *widen* pore throats, reduce capillary threshold pressures and increase connectivity (Figures 10c and 10d). In a fluid reservoir these rocks would form a poor fault seal, despite the volume of clay increasing in some faulted samples (Figures 7 and 10c). Authigenic chlorite is commonly present in many sandstone reservoirs, i.e., at depths of 3,000 m or more in the North Sea (Ziegler, 2006), with low concentrations of smectite and kaolinite as replacement minerals (Bjørlykke & Aagaard, 1992; Inoue et al., 1987; Nadeau et al., 1984) and in sandstones comprising lithics and mafic minerals (such as the volcanogenic sandstones of the Eumeralla Formation). When pore filling, authigenic chlorite is present in these relatively high abundances (i.e., >5% clay volume) it tends to have a large negative impact on permeability (Worden et al., 2020). Therefore, our results show that in chlorite clay-bearing reservoirs, rather than representing fluid bounding structures, some fault zones may actually form important fluid draining structures.

In contrast, compaction and shearing of authigenic kaolinite in fault zones causes some reduction in overall pore connectivity by decreasing pore throat size distribution and capillary threshold pressures relative to unfaulted samples (Figures 10a and 10b). Although porosities are reduced (by up to 25%), the magnitude of permeability in faulted samples adjacent to the fault surface is only slightly lower than in unfaulted host rock (Figure 8). The most pronounced role of faulted authigenic kaolinite on fault rock properties is the

development of aligned pore-filling clay fabrics (formed by low grade strain causing shearing of kaolinite "books") *contributing* to the anisotropic fluid pathways primarily formed from oriented secondary dissolution pores (Farrell & Healy, 2017). This is important because diagenetic-clay minerals in the North Sea fluvial and shallow marine sandstones are dominated by kaolinite, and as this clay can be crystallized at relatively low temperatures it is common in even shallow reservoirs (Bjørlykke & Aagaard, 1992). Therefore, compacted and sheared pore-filling kaolinites are likely to be found around faults in these reservoirs and could contribute to anisotropic fluid-flow in fault zones that influences capillary seal capacity. The faults sampled in this study are both inverted normal faults. Multiple phases of clay precipitation in faults with more complex histories including inversion, may be more likely to result in authigenic clays with several morphologies within a single fault rock.

5.3. Role of Faulted Authigenic Clays in Fault Seal Predictions

Previous studies have shown that the mineralogical composition and morphology of clays, derived from the natural habit of different phyllosilicate minerals, can contribute to permeability properties of unfaulted sandstones (Neasham, 1977). Deformation of clays is fundamental to reducing permeability around faults (Fisher & Knipe, 1998). Existing algorithms used to predict the sealing capacity of faults notionally include information on the composition of the seal or gouge, however "composition" describes the volume of clay which can be calculated from "shaliness" determined from gamma ray wireline logs rather than the mineralogical composition of the clay volume. By integrating clay mineralogy data with investigation methods from fault seal and gouge studies, this study has shown that the permeability properties of faulted sandstones are also related to clay morphologies. In this case, previously undescribed morphologies, produced by the deformation history of those clays: for example, cataclased chlorites and sheared kaolinites (Figure 13). These results indicate that incorporation of spectral gamma ray data to fault seal algorithms to identify specific clay types like kaolinite and illite would be useful for interpreting the likely petrophysical properties of a potential seal.

The role of clays in contributing to permeability patterns in fault seal and experimental fault gouge studies tend to focus on permeabilities of rocks directly adjacent to the fault surface, termed the fault core (Figure 13). In addition to highlighting the contribution of varying clay type/morphology to permeability, results from this study have advanced the scope of fault seal and fault gouge studies to consider the influence of clays on permeability patterns in fault-damaged rocks i.e., adjacent to the fault core in the fault damage zone (Figure 13). Development of effective seals capable of retaining differences in fluid levels and pressures across a fault is fundamentally dependent on an extensive and continuous low permeability surface or zone formed along the fault plane in the fault core. However capillary seal capacity is a dynamic property which is dependent on the fluid pressure differences in fault damage zone rocks adjacent to the seal. Enhanced fluid-flow in the damage zone (i.e., high permeabilities in the Eumeralla sandstone) may–over time–reduce pressure in the fluid trap, as the fluid-flows away in the direction of the pressure gradient (most likely up fault dip) leading to changes in sealing capacity. The development of anisotropic fluid-flow in damage zone rocks (i.e., anisotropy of permeability in the Scapa sandstone) could also accelerate this process. Identification of anisotropic fluid-flow and its impact on fault sealing capacity has previously been described in cataclased sandstones (Farrell et al., 2014) and fault gouge studies (Evans et al., 1997; Faulkner & Rutter, 2001). In these studies, permeabilities taken normal to the fault surface were five orders of magnitude lower permeabilities than cores oriented parallel to fault dip (Farrell et al., 2014). As most wellbore cores are sampled vertically, most core plugs are sampled sub-horizontal i.e., perpendicular to high angle faults. As shown in this study, permeabilities of 'normal to fault' oriented core plugs may be orders of magnitude lower than values from "parallel to fault dip" core plugs. Therefore, what apparently constitutes a "fault seal" in one direction may actually be a "fault drain" in another.

5.4. Further Work

Interpretation of the processes that have altered the morphology and distribution of kaolinite and chlorite in faulted sandstones has focused on structural deformation. However, fluid composition and temperature are intrinsic to the precipitation of authigenic clays and as well as being regionally controlled by burial depth, these variables can have a localized relationship to fault zones (Fisher & Knipe, 1998). For example,

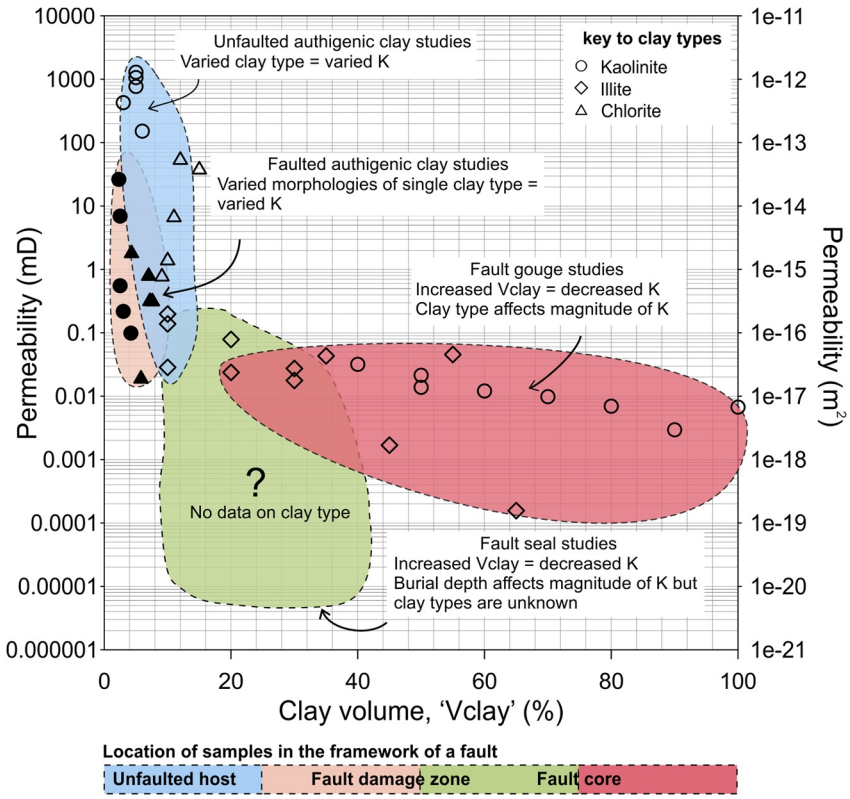

Figure 13. Graph summarizing the relationships between permeability and clay content identified in faulted sandstones (after Fisher & Knipe, 2001) from this study (filled symbols) and published studies (open symbols) investigating the role of clays on fluid-flow in: unfaulted sandstones (Neasham, 1977); faulted phyllosilicate-rich sandstones from fault damage zone/fault core (Fisher & Knipe, 2001; Sperrevik et al., 2000); and sandstone derived fault gouge from the fault core (Crawford et al., 2008; Gibson, 1998). Comparison with correlations drawn from previous studies indicates that clay mineralogy and morphology are more significant controls on permeability than Vclay in unfaulted host rocks and damage zone fault rocks.

XRD data from chlorite-rich sandstones show a change in the Fe ion content of chlorites between unfaulted (Fe^{3+}) and faulted samples (Fe^{2+}) which may make clays more soluble in acidic conditions. Speculation about the chemistry of fault related fluids and temperatures can be made, but with the data available, these samples can only present a static picture of the microstructure. Future work conducting experimental deformation on impure sandstones using controlled temperature, pressure and pore fluid compositions could provide additional insight into the conditions required for clay precipitation.

The use of gas as a pore fluid in this study has the following advantages: nitrogen gas is chemically inert, allowing geo-chemical effects to be ignored, so only permeability variation caused by change in confining pressure needs to be considered. Although the clays in this study are not swelling, the impact of using liquid as a pore fluid could include holding of irreducible water in micropores (Wilson & Pittman, 1977). In a subsurface reservoir setting with varied pore fluids (i.e., NaCl rich brines, acidic fluids) and combinations of gas and liquids, the effect of salinity and/or acidity will likely affect the wettability of all minerals but especially clays and the impact of this on permeability should be experimentally investigated.

This study contains novel information of the microstructure of deformed authigenic clays in naturally occurring faults. These authigenic minerals were formed by the breakdown of framework grains (feldspar and chlorite) and precipitation of clays. The *contribution* of clay morphologies on permeability cannot be quantified without a 'non-clay' portion of these sandstones, which do not exist naturally. Examples of studies which have isolated the effects of authigenic clays through clay destruction, modeling and synthetic sandstones conclude that authigenic clays have a significant effect on permeability (Howard, 1992;

Nadeau, 1998; Pallatt et al., 1984). It may be worthwhile to deform synthetic versions of porous sandstones containing controlled amounts of authigenic clays in the laboratory.

6. Conclusions

In summary, we present novel microstructural and petrophysical results showing that tectonic deformation can alter the morphology and distribution of pore residing authigenic clays and that these changes can alter the petrophysical properties of faulted impure sandstones. Microstructural analysis has shown that, as well as varying the volume of pore space (fracturing and dissolution of framework grains and compaction), fault deformation can vary the morphology, aggregate structure and distribution of authigenic kaolinite within macropores, directly *contributing* to formation of anisotropic permeability pathways (through shearing of tightly packed and sheared kaolinite "books"). Results have also shown that deformation driven cataclasis of authigenic chlorites can break-up the pore lining distribution into dispersed clumps of clay with reduced crystal size. In contrast to the effect of faulting on authigenic kaolinite, in the case of chlorite, cataclasis has opened pore throats and enhanced permeability. While wireline log data can help to estimate fault zone "shaliness" and calculate the volume of clay to interpret fault seal in impure sandstones, our results demonstrate the strong influence of fault related authigenic clays on fluid-flow around faults and highlights the value of incorporating information about different clay types into fault seal models.

While previous studies have observed variations in permeability due to distinctive morphologies of different authigenic clays in unfaulted sandstones (Neasham, 1977), this study advances these findings by showing that fault deformation can generate varying fabrics and morphologies in a single type of authigenic clay, which contribute to permeability trends not previously reported around faults in impure sandstones. These novel results prompt questions about the robustness of parameters currently used to model fluid-flow around faults in sandstones containing authigenic clays and should motivate geologists and rock physicists to take a fresh look at fault seal analysis in impure sandstones.

Data Availability Statement

The petrophysical and geochemical data published in this study are available on Figshare: 10.6084/m9.figshare.9633527. v1 and 10.6084/m9. figshare.9633524. v1.

Acknowledgments
Thanks to John Still and Alex Brasier for access to the ACEMAC SEM at the University of Aberdeen; Lorenza Sardisco and Jonathan Wilkens at X-ray minerals for XRD analysis; Editor Douglas Schmitt, Associate Editor Mike Heap, Prof. Ben van der Pluijm, Prof. Jim Evans, Prof. Fabrizio Balsamo and three anonymous reviewers for encouraging and constructive reviews. This work forms part of a UKRI/NERC-funded project on the anisotropy of permeability (NE/N003063/1).

References

Antonellini, M., & Aydin, A. (1994). Effect of faulting on fluid-flow in porous sandstones: Petrophysical properties. *AAPG Bulletin*, *78*(3), 355–377. https://doi.org/10.1306/bdff90aa-1718-11d7-8645000102c1865d

Bjørlykke, K. (1998). Clay mineral diagenesis in sedimentary basins—A key to the prediction of rock properties. Examples from the North Sea Basin. *Clay Minerals*, *33*(1), 15–34.

Bjørlykke, K., & Aagaard, P. (1992). Clay minerals in North Sea sandstones.

Bjørlykke, K., & Jahren, J. (2012). Open or closed geochemical systems during diagenesis in sedimentary basins: Constraints on mass transfer during diagenesis and the prediction of porosity in sandstone and carbonate reservoirsGeohorizon. *AAPG Bulletin*, *96*(12), 2193–2214.

Bushell, T. P. (1986). Reservoir geology of the Morecambe Field. *Geological Society, London, Special Publications*, *23*(1), 189–208. https://doi.org/10.1144/gsl.sp.1986.023.01.12

Childs, C., Walsh, J. J., & Watterson, J. (1997). Complexity in fault zone structure and implications for fault seal prediction. In *Norwegian petroleum society special publications* (Vol. 7, pp. 61–72). Elsevier. https://doi.org/10.1016/s0928-8937(97)80007-0

Crawford, B. R., Faulkner, D. R., & Rutter, E. H. (2008). Strength, porosity, and permeability development during hydrostatic and shear loading of synthetic quartz-clay fault gouge. *Journal of Geophysical Research*, *113*(B3), B03207. https://doi.org/10.1029/2006JB004634

De Waal, J. A., Bil, K. J., Dicker, A. I. M., & Kantorowicz, J. D. (1988). Petrophysical core analysis of sandstones containing delicate illite. *Log Analyst*, *29*(05). Paper number: SPWLA-1988-v29n5a1.

Debenham, N., Farrell, N. J., Holford, S. P., King, R. C., & Healy, D. (2019). Spatial distribution of micrometre-scale porosity and permeability across the damage zone of a reverse-reactivated normal fault in a tight sandstone: Insights from the Otway Basin, SE Australia. *Basin Research*, *31*(3), 640–658. https://doi.org/10.1111/bre.12345

Debenham, N., King, R. C., & Holford, S. P. (2018). The influence of a reverse-reactivated normal fault on natural fracture geometries and relative chronologies at Castle Cove, Otway Basin. *Journal of Structural Geology*, *112*, 112–130. https://doi.org/10.1016/j.jsg.2018.05.004

Derjaguin, B. V., Churaev, N. V., Muller, V. M., & Kisin, V. I. (1987). *Surface forces*. Consultants Bureau.

Duddy, I. R. (2003). Mesozoic: A time of change in tectonic regime. In *Geology of Victoria* (Vol. 23, pp. 239–286). Geological Society of Australia Victoria Division.

Eichhubl, P., D'Onfro, P. S., Aydin, A., Waters, J., & McCarty, D. K. (2005). Structure, petrophysics, and diagenesis of shale entrained along a normal fault at Black Diamond Mines, California—Implications for fault seal. *AAPG Bulletin*, *89*(9), 1113–1137. https://doi.org/10.1306/04220504099

Evans, J. P., Forster, C. B., & Goddard, J. V. (1997). Permeability of fault-related rocks, and implications for hydraulic structure of fault zones. *Journal of Structural Geology*, *19*(11), 1393–1404. https://doi.org/10.1016/s0191-8141(97)00057-6

Farrell, N. J. C., & Healy, D. (2017). Anisotropic pore fabrics in faulted porous sandstones. *Journal of Structural Geology*, *104*, 125–141. https://doi.org/10.1016/j.jsg.2017.09.010

Farrell, N. J. C., Healy, D., & Taylor, C. W. (2014). Anisotropy of permeability in faulted porous sandstones. *Journal of Structural Geology*, *63*, 50–67. https://doi.org/10.1016/j.jsg.2014.02.008

Faulkner, D. R., & Rutter, E. H. (1998). The gas permeability of clay-bearing fault gouge at 20°C. *Geological Society, London, Special Publications*, *147*(1), 147–156. https://doi.org/10.1144/gsl.sp.1998.147.01.10

Faulkner, D. R., & Rutter, E. H. (2001). Can the maintenance of overpressured fluids in large strike-slip fault zones explain their apparent weakness? *Geology*, *29*(6), 503–506. https://doi.org/10.1130/0091-7613(2001)029<0503:ctmoof>2.0.co;2

Fisher, Q. J., & Knipe, R. (1998). Fault sealing processes in siliciclastic sediments. *Geological Society, London, Special Publications*, *147*(1), 117–134. https://doi.org/10.1144/gsl.sp.1998.147.01.08

Fisher, Q. J., & Knipe, R. J. (2001). The permeability of faults within siliciclastic petroleum reservoirs of the North Sea and Norwegian Continental Shelf. *Marine and Petroleum Geology*, *18*(10), 1063–1081. https://doi.org/10.1016/s0264-8172(01)00042-3

Fowles, J., & Burley, S. (1994). Textural and permeability characteristics of faulted, high porosity sandstones. *Marine and Petroleum Geology*, *11*(5), 608–623. https://doi.org/10.1016/0264-8172(94)90071-x

Freeman, B., Yielding, G., Needham, D. T., & Badley, M. E. (1998). Fault seal prediction: The gouge ratio method. *Geological Society, London, Special Publications*, *127*(1), 19–25. https://doi.org/10.1144/gsl.sp.1998.127.01.03

Fristad, T. A. G. B. P., Groth, A., Yielding, G., & Freeman, B. (1997). Quantitative fault seal prediction: A case study from Oseberg Syd. In *Norwegian petroleum society special publications* (Vol. 7, pp. 107–124). Elsevier.

Fulljames, J. R., Zijerveld, L. J. J., & Franssen, R. C. M. W. (1997). Fault seal processes: Systematic analysis of fault seals over geological and production time scales. In *Norwegian petroleum society special publications* (Vol. 7, pp. 51–59). Elsevier. https://doi.org/10.1016/s0928-8937(97)80006-9

Gibson, R. G. (1998). Physical character and fluid-flow properties of sandstone-derived fault zones. *Geological Society, London, Special Publications*, *127*(1), 83–97. https://doi.org/10.1144/gsl.sp.1998.127.01.07

Haines, S. H., Van Der Pluijm, B. A., Ikari, M. J., Saffer, D. M., & Marone, C. (2009). Clay fabric intensity in natural and artificial fault gouges: Implications for brittle fault zone processes and sedimentary basin clay fabric evolution. *Journal of Geophysical Research*, *114*(B5), B05406. https://doi.org/10.1029/2008JB005866

Heaviside, J., & Black, C. J. J. (1983). Fundamentals of relative permeability: Experimental and theoretical considerations. In *SPE annual technical conference and exhibition*. OnePetro.

Hippler, S. J. (1993). Deformation microstructures and diagenesis in sandstone adjacent to an extensional fault: Implications for the flow and entrapment of hydrocarbons. *AAPG Bulletin*, *77*(4), 625–637. https://doi.org/10.1306/bdff8cb8-1718-11d7-8645000102c1865d

Howard, J. J. (1992). Influence of authigenic-clay minerals on permeability.

Hurst, A., & Nadeau, P. H. (1995). Clay microporosity in reservoir sandstones: An application of quantitative electron microscopy in petrophysical evaluation. *AAPG Bulletin*, *79*(4), 563–573. https://doi.org/10.1306/8d2b1598-171e-11d7-8645000102c1865d

Inoue, A., Kohyama, N., Kitagawa, R., & Watanabe, T. (1987). Chemical and morphological evidence for the conversion of smectite to illite. *Clays and Clay Minerals*, *35*(2), 111–120. https://doi.org/10.1346/ccmn.1987.0350203

Jolley, S. J., Dijk, H., Lamens, J. H., Fisher, Q. J., Manzocchi, T., Eikmans, H., & Huang, Y. (2007). Faulting and fault sealing in production simulation models: Brent Province, northern North Sea. *Petroleum Geoscience*, *13*(4), 321–340. https://doi.org/10.1144/1354-079306-733

Jones, F. O., & Owens, W. W. (1980). A laboratory study of low-permeability gas sands. *Journal of petroleum Technology*, *32*(09), 1–631. https://doi.org/10.2118/7551-pa

Kantorowicz, J. D. (1990). The influence of variations in illite morphology on the permeability of Middle Jurassic Brent Group sandstones, Cormorant Field, UK North Sea. *Marine and Petroleum Geology*, *7*(1), 66–74. https://doi.org/10.1016/0264-8172(90)90057-n

Klinkenberg, L. J. (1941). The permeability of porous media to liquids and gases. In *Drilling and production practice*. OnePetro.

Knipe, R. J. (1992). Faulting processes and fault seal. In *Structural and tectonic modelling and its application to petroleum geology* (pp. 325–342). Elsevier. https://doi.org/10.1016/b978-0-444-88607-1.50027-9

Knipe, R. J. (1997). Juxtaposition and seal diagrams to help analyze fault seals in hydrocarbon reservoirs. *AAPG Bulletin*, *81*(2), 187–195.

Knott, S. D. (1993). Fault seal analysis in the North Sea. *AAPG Bulletin*, *77*, 778–792. https://doi.org/10.1306/bdff8d58-1718-11d7-8645000102c1865d

Krassay, A. A., Cathro, D. L., Ryan, D. J., Boult, P. J., Johns, D. R., & Lang, S. C. (2004). A regional tectonostratigraphic framework for the Otway Basin.

Lanson, B., Beaufort, D., Berger, G., Bauer, A., Cassagnabere, A., & Meunier, A. (2002). Authigenic kaolin and illitic minerals during burial diagenesis of sandstones: A review. *Clay Minerals*, *37*(1), 1–22. https://doi.org/10.1180/0009855023710014

Lanson, B., Sakharov, B. A., Claret, F., & Drits, V. A. (2009). Diagenetic smectite-to-illite transition in clay-rich sediments: A reappraisal of X-ray diffraction results using the multi-specimen method. *American Journal of Science*, *309*(6), 476–516. https://doi.org/10.2475/06.2009.03

Laubach, S. E., Eichhubl, P., Hargrove, P., Ellis, M. A., & Hooker, J. N. (2014). Fault core and damage zone fracture attributes vary along strike owing to interaction of fracture growth, quartz accumulation, and differing sandstone composition. *Journal of Structural Geology*, *68*, 207–226. https://doi.org/10.1016/j.jsg.2014.08.007

Lindsay, N. G., Murphy, F. C., Walsh, J. J., Watterson, J., Flint, S., & Bryant, I. (1993). Outcrop studies of shale smears on fault surfaces. *The geological modelling of hydrocarbon reservoirs and outcrop analogues*, *15*, 113–123.

Lommatzsch, M., Exner, U., Gier, S., & Grasemann, B. (2015). Structural and chemical controls of deformation bands on fluid-flow: Interplay between cataclasis and diagenetic alteration. *AAPG Bulletin*, *99*(4), 689–710. https://doi.org/10.1306/10081413162

Manzocchi, T., Walsh, J. J., Nell, P., & Yielding, G. (1999). Fault transmissibility multipliers for flow simulation models. *Petroleum Geoscience*, *5*(1), 53–63. https://doi.org/10.1144/petgeo.5.1.53

Milliken, K. L. (2001). Diagenetic heterogeneity in sandstone at the outcrop scale, Breathitt Formation (Pennsylvanian), eastern Kentucky. *AAPG Bulletin*, *85*(5), 795–815. https://doi.org/10.1306/8626ca05-173b-11d7-8645000102c1865d

Moore, D. M., & Reynolds, R. C., Jr. (1989). *X-ray diffraction and the identification and analysis of clay minerals* (p. 378). Oxford University Press.

Morrow, C. A., Shi, L. Q., & Byerlee, J. D. (1984). Permeability of fault gouge under confining pressure and shear stress. *Journal of Geophysical Research*, *89*(B5), 3193–3200. https://doi.org/10.1029/jb089ib05p03193

Nadeau, P. H. (1998). An experimental study of the effects of diagenetic clay minerals on reservoir sands. *Clays and Clay Minerals*, *46*(1), 18–26. https://doi.org/10.1346/ccmn.1998.0460103

Nadeau, P. H., & Hurst, A. (1991). Application of back-scattered electron microscopy to the quantification of clay mineral microporosity in sandstones. *Journal of Sedimentary Research*, *61*(6), 921–925. https://doi.org/10.1306/d4267807-2b26-11d7-8648000102c1865d

Nadeau, P. H., Wilson, M. J., McHardy, W. J., & Tait, J. M. (1984). Interstratified clays as fundamental particles. *Science*, *225*(4665), 923–925. https://doi.org/10.1126/science.225.4665.923

Neasham, J. W. (1977). The morphology of dispersed clay in sandstone reservoirs and its effect on sandstone shaliness, pore space and fluid-flow properties. In *SPE annual fall technical conference and exhibition*. Society of Petroleum Engineers. OnePetro. Paper Number: SPE-6858-MS. https://doi.org/10.2118/6858-ms

Pallatt, N., Wilson, M. J., & McHardy, W. J. (1984). The relationship between permeability and the morphology of diagenetic illite in reservoir rocks. *Journal of Petroleum Geology*, *36*, 2225–2227. https://doi.org/10.2118/12798-pa

Pike, J. D. (1981). Feldspar diagenesis in the Yowlumne sandstone Kern County, California (132 p). Texas A&M University, M.S. thesis.

Rempe, M., Mitchell, T. M., Renner, J., Smith, S. A., Bistacchi, A., & Di Toro, G. (2018). The relationship between microfracture damage and the physical properties of fault-related rocks: The Gole Larghe Fault Zone, Italian Southern Alps. *Journal of Geophysical Research: Solid Earth*, *123*(9), 7661–7687. https://doi.org/10.1029/2018jb015900

Schlumberger (2016). The Defining Series: Formation damage. Oilfield Review. Retrieved from https://www.slb.com/resource-library/oilfield-review/defining-series/defining-formation-damage

Schowalter, T. T. (1979). Mechanics of secondary hydrocarbon migration and entrapment. *AAPG Bulletin*, *63*(5), 723–760. https://doi.org/10.1306/2f9182ca-16ce-11d7-8645000102c1865d

Sperrevik, S., Færseth, R. B., & Gabrielsen, R. H. (2000). Experiments on clay smear formation along faults. *Petroleum Geoscience*, *6*(2), 113–123. https://doi.org/10.1144/petgeo.6.2.113

Stalder, P. J. (1973). Influence of crystallographic habit and aggregates structure on sandstone permeability. *Geologie Mignbouw*, *52*, 217–222.

Swanson, B. F. (1981). A simple correlation between permeabilities and mercury capillary pressures. *Journal of Petroleum Technology*, *33*(12), 2–498. https://doi.org/10.2118/8234-pa

Tanikawa, W., & Shimamoto, T. (2009). Comparison of Klinkenberg-corrected gas permeability and water permeability in sedimentary rocks. *International Journal of Rock Mechanics and Mining Sciences*, *46*(2), 229–238. https://doi.org/10.1016/j.ijrmms.2008.03.004

Thomas, J. B. (1978). Diagenetic sequences in low-permeability argillaceous sandstones. *Journal of the Geological Society*, *135*(1), 93–99. https://doi.org/10.1144/gsjgs.135.1.0093

Thomeer, J. H. M. (1960). Introduction of a pore geometrical factor defined by the capillary pressure curve. *Journal of Petroleum Technology*, *12*(03), 73–77. https://doi.org/10.2118/1324-g

Vrolijk, P. J., Urai, J. L., & Kettermann, M. (2016). Clay smear: Review of mechanisms and applications. *Journal of Structural Geology*, *86*, 95–152. https://doi.org/10.1016/j.jsg.2015.09.006

Washburn, E. W. (1921). The dynamics of capillary flow. *Physical review*, *17*(3), 273–283. https://doi.org/10.1103/physrev.17.273

Wilson, M. D., & Pittman, E. D. (1977). Authigenic clays in sandstones; recognition and influence on reservoir properties and paleoenvironmental analysis. *Journal of Sedimentary Research*, *47*(1), 3–31. https://doi.org/10.1306/212f70e5-2b24-11d7-8648000102c1865d

Wilson, M. J., Deer, W. A., Howie, R. A., & Zussman, J. (2013). Rock-forming minerals, volume 3C, Sheet silicates: Clay minerals. Geological Society.

Wilson, M. J., Wilson, L., & Patey, I. (2014). The influence of individual clay minerals on formation damage of reservoir sandstones: A critical review with some new insights. *Clay Minerals*, *49*(2), 147–164. https://doi.org/10.1180/claymin.2014.049.2.02

Worden, R. H., Griffiths, J., Wooldridge, L. J., Utley, J. E. P., Lawan, A. Y., Muhammed, D. D., et al. (2020). Chlorite in sandstones. *Earth-Science Reviews*, *204*, 103105. https://doi.org/10.1016/j.earscirev.2020.103105

Worden, R. H., & Morad, S. (1999). Clay minerals in sandstones: Controls on formation, distribution and evolution. *Clay mineral cements in sandstones* (pp. 1–41).

Yielding, G. (2002). Shale Gouge ratio—Calibration by geohistory. In *Norwegian petroleum society special publications* (Vol. 11, pp. 1–15). Elsevier. https://doi.org/10.1016/s0928-8937(02)80003-0

Yielding, G., Freeman, B., & Needham, D. T. (1997). Quantitative fault seal prediction. *AAPG Bulletin*, *81*(6), 897–917. https://doi.org/10.1306/522b498d-1727-11d7-8645000102c1865d

Zhang, S., & Cox, S. F. (2000). Enhancement of fluid permeability during shear deformation of a synthetic mud. *Journal of Structural Geology*, *22*(10), 1385–1393. https://doi.org/10.1016/s0191-8141(00)00065-1

Ziegler, K. (2006). Clay minerals of the Permian Rotliegend Group in the North Sea and adjacent areas. *Clay Minerals*, *41*, 355–393. https://doi.org/10.1180/0009855064110200

Reference From the Supporting Information

Wu, Y. S., & Pruess, K. (1998). Gas flow in porous media with Klinkenberg effects. *Transport in Porous Media*, *32*(1), 117–137.